Chapter

Mechanisms of Photoisomerization and Water Oxidation Catalysis of Ruthenium (II) Aquo Complexes

Yuta Tsubonouchi, Eman A. Mohamed, Zaki N. Zahran and Masayuki Yagi

Abstract

Polypyridyl ruthenium(II) complexes have been widely researched as promising functional molecules. We have found unique photoisomerization reactions of polypyridyl ruthenium(II) aquo complexes. Recently we have attempted to provide insight into the mechanism of the photoisomerization of the complexes and distinguish between the *distal*−/*proximal*-isomers in their physicochemical properties and functions. Moreover, polypyridyl ruthenium(II) aquo complexes have been intensively studied as active water oxidation catalysts (WOCs) which are indispensable for artificial photosynthesis. The catalytic aspect and mechanism of water oxidation by the *distal*-/*proximal*-isomers of polypyridyl ruthenium(II) aquo complexes have been investigated to provide the guided thought to develop more efficient molecular catalysts for water oxidation. The recent progress on the photoisomerization and water oxidation of polypyridyl ruthenium(II) aquo complexes in our group are reviewed to understand the properties and functions of ruthenium complexes.

Keywords: Ruthenium aquo complexes, Photoisomerization, Water oxidation catalysis, Artificial photosynthesis

1. Introduction

Polypyridyl ruthenium(II) complexes have been widely researched as promising functional molecules due to appealing photochemical [1–3] and photophysical [4–6] properties as well as redox properties [7, 8], which enable them to exhibit a number of functions such as electrochromism [9, 10], proton-coupled electron transfer [11–13] and photocatalysis [14, 15]. As a result, the polypyridyl ruthenium(II) complexes have been applied to a large variety of devices including sensors [16], photovoltaic cells [17], displays [18] and artificial photosynthesis [19, 20].

We presented irreversible and stoichiometric photoisomerization of *distal*-$[Ru(tpy)(pynp)OH_2]^{2+}$ (*d*-**1**) (tpy = 2,2′;6′,2″-terpyridine, pynp = 2-(2-pyridyl)-1,8-naphthyridine) to *proximal*-$[Ru(tpy)(pynp)OH_2]^{2+}$ (*p*-**1**) as shown in **Figure 1** [21–23], which had not been characterized previously for polypyridyl ruthenium

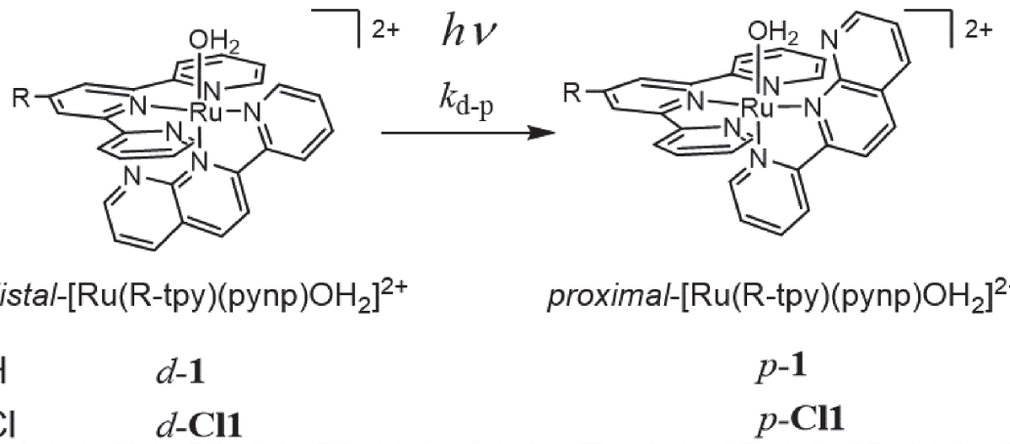

Figure 1.
Photoisomerization of distal-*[Ru(Rtpy)(pynp)OH₂]²⁺ to* proximal-*isomers.*

(II) aquo complexes although various photochemical reactions of the ruthenium(II) complexes have been reported [24–33]. We have attempted to provide insight into the mechanism of the photoisomerization of polypyridyl ruthenium(II) aquo complexes and distinguish between the *distal−/proximal*-isomers in their physicochemical properties and functions [21–23, 34–36]. We have also developed new synthetic strategy to form dinuclear ruthenium(II) complexes utilizing the photoisomerization [37, 38]. Moreover, polypyridyl ruthenium(II) aquo complexes have been intensively studied as active WOCs [21, 22, 34, 35, 37, 39, 40] which are indispensable for artificial photosynthesis. The catalytic aspect and mechanism of water oxidation by the *distal-/proximal*-isomers of polypyridyl ruthenium(II) aquo complexes have been investigated to provide the guided thought to develop more efficient molecular catalysts for water oxidation. In this chapter, we review the recent progress on the photoisomerization and water oxidation of polypyridyl ruthenium(II) aquo complexes in our group.

2. Photoisomerization of polypyridyl ruthenium(II) aquo complexes

With respect to the photoisomerization of polypyridyl Ru(II) aquo complexes, the photoisomerization of *cis*-$[Ru(bpy)_2(OH_2)_2]^{2+}$ (bpy = 2,2′-bipyridine) to its trans form in aqueous media was first reported by Meyer [24]. The mechanism of the photoisomerization reaction was later investigated by Planas et al. [41]. In this case, the *trans* form was present as a photostationary state and slowly went back to the original *cis* form. To the best of our knowledge, the *cis*-$[Ru(bpy)_2(OH_2)_2]^{2+}$ had been the only one polypyridyl Ru(II) aquo complex that exhibits photoisomerization behavior before we presented the photoisomerization of *d*-**1** to *p*-**1** [21]. Furthermore, we reported the reversible photoisomerization equilibrium between *distal- and proximal*-$[Ru(tpy)(pyqu)OH_2]^{2+}$ (*d*-**2** and *p*-**2**) isomers with a ligand of 2-(2-pyridyl)quinoline (pyqu) instead of pynp, in contrast to the irreversible photoisomerization of *d*-**1** to *p*-**1**. The aspect and mechanism of the irreversible photoisomerization of *d*-**1** are first described, followed by those of the reversible one of *d−/p*-**2** in this section.

2.1 Irreversible photoisomerization of *distal*-$[Ru(Xtpy)(pynp)OH_2]^{2+}$ to the *proximal*-isomer

Photoisomerization behavior of *d*-**1** was investigated by ^{1}H-NMR and UV–Vis spectroscopy. Upon irradiation of visible light to a D_2O solution of *d*-**1**, the NMR

peak at 9.6 ppm due to *d*-**1** decreased with the irradiation time and disappeared completely after 25 min under the experimental conditions (**Figure 2A**) [21]. The new peak at 8.9 ppm assigned to *p*-**1** increased with the concomitant decrease of *d*-**1**. **Figure 2B** displays the concentration profile of *d*-**1** and *p*-**1**, which indicates that irreversible and stoichiometric photoisomerization from *d*-**1** to *p*-**1** proceeds in water by visible light irradiation (**Figure 1**). By contrast, no isomerization of *d*-**1** in water was found to occur under thermal treatment. The photoisomerization rate showed a first-order dependence on *d*-**1** concentration, and the kinetic analysis provided the observed rate constant ($(k_{d\text{-}p})_{obs}/s^{-1}$) of photoisomerization (*distal* to *proximal*) to be 4.1 x 10^{-3} s^{-1} under the conditions employed ($\lambda > 420$ nm, 180 mW cm^{-2}). The $(k_{d\text{-}p})_{obs}$ values increased linearly with respect to the light intensity below 255 mW cm^{-2}, indicating that the photoexcited state participated in photoisomerization under the employed conditions. Arrhenius plots of the photoisomerization gave a straight line in a range of 10 ~ 35°C, providing 41.7 kJ mol^{-1} of activation energy (E_a) for the photoisomerization (**Table 1**). Interestingly, the $(k_{d\text{-}p})_{obs}$ value decreased drastically at pD > 7 (pD = −log [D^+]), while it was unchanged over pD 1-7. The UV–Vis spectrophotometric pH titration of *d*-**1** gave pK_a of 9.7 attributed to the deprotonation of an aquo ligand to form the hydroxo complex, *distal*-[Ru(tpy)(pynp)OH]$^+$. The trend of $(k_{d\text{-}p})_{obs}$ change depending on pH corresponds to the fraction of *d*-**1** (aquo form) dissolved in the solution versus pH, suggesting that the hydroxo form of *d*-**1** is inert for the photoisomerization [21, 22].

The internal quantum yield (Φ) for photoisomerization, which is defined as the ratio of the number of the photoisomerized complexes to the number of incident photons of a given energy, was estimated from the UV–vis spectral change in the experiment under monochromatic light irradiation (520 nm, 26.4 mW cm^{-2}). The Φ values were calculated according to the following equation:

$$\Phi = \frac{hcN_A k_{pi} n_{int}}{p\lambda A(1\text{-}T)} \quad (1)$$

where h, c, N_A, k_{pi}, n_{int}, p, λ, A and T are Plank's constant, the speed of light, Avogadro's number, the rate constant for photoisomerization, initial amount of the complex, photon flux, wavelength, the irradiated area and the transmittance,

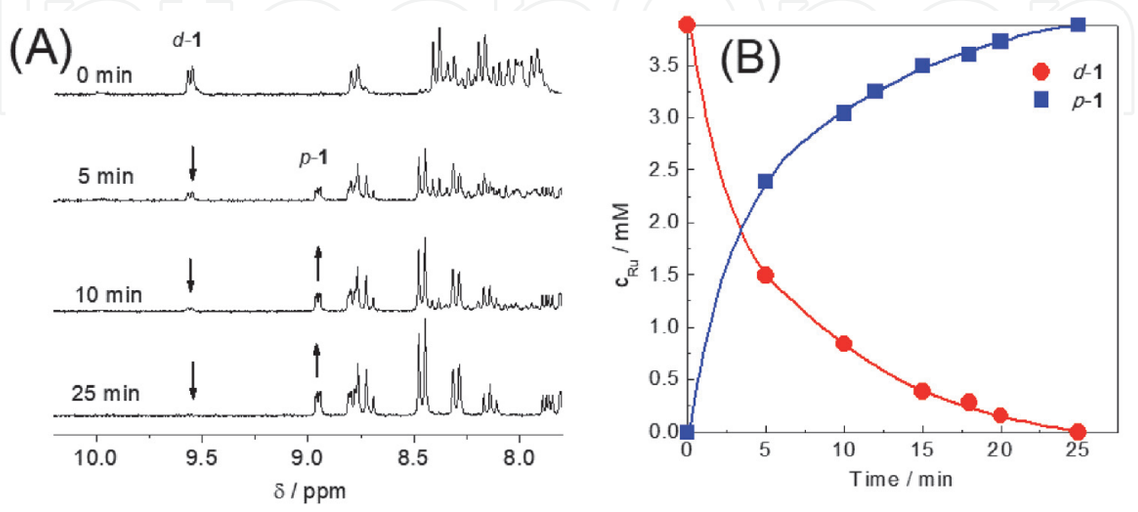

Figure 2.
(A) Time course of ^{1}H NMR spectral changes during the photoisomerization of d-**1** *in D_2O with 180 mW cm^{-2} visible light irradiation ($\lambda > 420$ nm). (B) Kinetic profiles of* d-**1** *(red circle) and of* p-**1** *(blue square). (Reproduced with permission of American Chemical Society from ref. [21]).*

Complexes	λ_{max} / nm (ε / M^{-1} cm^{-1})	pK_a	c_{Ru} / mM	Photoisomerization parameters				Ref.
				$(k_{d\text{-}p})_{obs}$ / s^{-1b}	$(k_{p\text{-}d})_{obs}$ / s^{-1b}	Φ / % (λ = 520 nm)	E_a / kJ mol^{-1}	
d-**1**	527 (9,300)	9.7	0.088	n.m.	—	1.5	n.m.	[21]
			3.9	4.1×10^{-3}	—	0.31	41.7	[34]
p-**1**	524 (9,300)	10.7	3.9	—	n.r	—	—	[21]
d-**Cl1**	524 (8,600)	9.3	0.088	n.m.	—	2.1	n.m.	[35]
			3.9	4.9×10^{-3}	—	n.m.	n.m.	
p-**Cl1**	518 (8,900)	10.9	3.9	—	n.r	—	—	[35]
d-**2**	501 (8,300)	9.4	3.9	1.2×10^{-2}	—	1.1	23.3	[34]
p-**2**	502 (8,700)	10.5	3.9	—	4.3×10^{-3}	0.34	30.6	[34]
d-**3**	614 (5,700)	n.m.	2.0	n.m.	—	0.05	n.m.	[37]
p-**3**	612 (6,200)	n.m.	—	n.m.	n.m.	n.m.	n.m.	[37]

[a] c_{Ru} *is concentrations of ruthenium complexes. The marks of "n.m." and "n.r." mean "not measured" and "no reaction", respectively.*
[b] *The filtered halogen lamp was used for visible light irradiation (λ > 420 nm, 180 mW cm^{-2}).*

Table 1.
Summary of the observed rate constants and internal quantum yields of photoisomerization of d−/p-***1***, d−/p-***Cl1***, d−/p-***2*** *and* d−/p-***3*** *isomers at 25°C.*[a]

respectively. The Φ values for photoisomerization from *d*-**1** to *p*-**1** are 1.5 and 0.31% at 0.088 and 3.9 mM, respectively, as shown in **Table 1**.

In order to investigate influence of chloro substituent on photoisomerization of *d*-**1**, *distal*- and *proximal*-$[Ru(Cl\text{-}tpy)(pynp)OH_2]^{2+}$ (*d*-**Cl1** and *p*-**Cl1**; Cl-tpy = 4′-chloro-2,2′;6′,2″-terpyridine) complexes were prepared. When an aqueous solution of *d*-**Cl1** was irradiated with visible light (λ > 420 nm, 180 $mWcm^{-2}$), the stoichiometric photoisomerization of *d*-**Cl1** to *p*-**Cl1** was observed as it is for *d*-**1** (**Figure 1**). The rate constant for photoisomerization of *d*-**Cl1** was estimated to be $(k_{d\text{-}p})_{obs}$ = 4.9×10^{-3} s^{-1} [35], which is higher than that ($(k_{d\text{-}p})_{obs}$ = 4.1×10^{-3} s^{-1}) [22, 34] observed for *d*-**1** under the same conditions (**Table 1**). Additionally, the Φ value of *d*-**Cl1** (2.1%) is higher than that (Φ =1.5%) of *d*-**1**.

Several groups reported that some polypyridyl complexes undergo photosubstitution reactions *via* the triplet metal centered (^{3}MC) state from the ^{3}MLCT excited state [25–27]. According to the reports, a possible mechanism for the photoisomerization of *d*-**1** and *p*-**1** isomers was speculated as follows. The ^{3}MLCT excited state of *d*-**1** is generated by absorption of visible light. The photodissociation of the aquo ligand from the exited *d*-**1** proceeds through the thermal accessible ^{3}MC state, leading to the formation of the penta-coordinated $[Ru(tpy)(pynp)]^{2+}$ intermediate. The *p*-**1** isomer is formed by re-coordination of a water molecule to the penta-coordinated intermediate from the opposite direction of a tpy plane. The temperature-dependent transient absorption spectroscopic measurements of *d*-**1** suggest existence of the thermally activated process from the ^{3}MLCT state with an E_a of 49 kJ mol^{-1} [22], which is close to those from the ^{3}MLCT state to the ^{3}MC state reported for various polypyridyl Ru complexes [42–45]. The agreement of the E_a value (49 kJ mol^{-1}) with that (41.7 kJ mol^{-1}) calculated from the Arrhenius plot for the photoisomerization (**Table 1**) also supports the possibility that a main activation process of the photoisomerization reaction is the thermal transition from the ^{3}MLCT state to the ^{3}MC state. However, Density functional

theory (DFT) calculations suggested a different activation process, where the *distal*-penta-coordinated intermediate changes the conformation to *proximal*-penta-coordinated intermediate for *p*-**1** while maintaining the otherwise octahedral structure of *d*-**1** [22].

To obtain deeper mechanistic insights into the irreversible photoisomerization, the ^{3}MLCT excited states of the *d*-**1** and *p*-**1** were characterized by the time-resolved infrared spectroscopy (TR-IR) [36]. The decay of the photoexcited ^{3}MLCT states for both isomers were investigated by the TR-IR analysis, and the lifetimes of the excited state for the *d*-**1** and *p*-**1** were determined to be 9.7 ns and 6.4 ps, respectively. In general, the decay of the ^{3}MLCT excited states of Ru polypyridyl complexes occurs on nanosecond timescale or above, because the transition from a triplet excited state to a singlet ground state is forbidden by spin selection rules. The very short excited lifetime (6.4 ps) for *p*-**1** imply that a non-radiative process from the ^{3}MLCT state was accelerated, so that *p*-**1** is inert for photoisomerization to *d*-**1**.

The large difference in lifetimes of the ^{3}MLCT state between *d*-**1** and *p*-**1** was interpreted by geometry optimization calculations using DFT of both *d*-**1** and *p*-**1** isomers in the singlet ground (S_0) and ^{3}MLCT (T_1) states. While both the structures of *d*-**1** and *p*-**1** isomers in the S_0 states (indicated by lighter color atoms in **Figure 3**) show no considerable distortion, the aquo ligand was restricted by a hydrogen bond (1.48 Å) between its H atom and an N atom on the pynp ligand for *p*-**1**. The transition from S_0 state to T_1 state of *d*-**1** results in a significant change in the dihedral angle of the pynp plane to the tpy plane from 180° to 161°, together with bending at the bond between the naphthyridine and pyridine rings. The distortion for *d*-**1** is likely to originate from the steric hindrance between the extended π*-orbital of the pynp ligand and the π-orbital of the tpy ligand owing to the charge localization on the pynp ligand in the T_1 state. In the case of *p*-**1**, on the other hand, no considerable distortion was observed in the transition (**Figure 3**), but the Ru-O (1.98 Å) and hydrogen bonds (1.06 Å) between the pynp and the water ligands were shorter compared with the Ru-O (2.12 Å) and hydrogen bonds (1.48 Å) in the S_0 state. The shortened hydrogen bond is attributed to the charge localization on the pynp ligand in the T_1 state.

Figure 4 shows the DFT-calculated energy diagram of *d*-**1** and *p*-**1** in the S_0, T_1 and putative ^{3}MC states. *p*-**1** in the S_0 state is more stable than *d*-**1** by 65 kJ mol^{-1} because of hydrogen bond interaction between the pynp and the aquo ligand. The energy difference between the S_0 and T_1 states for *d*-**1** is 176 kJ mol^{-1}, which is remarkably higher than that (101 kJ mol^{-1}) for *p*-**1**. The higher energy difference for *d*-**1** is mainly due to the significant distortion of the pynp ligand on the transition from the S_0 to T_1 states (**Figure 3**). As a result, the energy of *d*-**1** in the T_1 state is higher than that of *p*-**1** in the T_1 state by 140 kJ mol^{-1}. Considering the similar ligand field for both isomers, the energy difference in the ^{3}MC state between *d*-**1** and *p*-**1** is assumed to be not as much as that (140 kJ mol^{-1}) in T_1 states. For *p*-**1**, the ^{3}MC state is presumed to be located at much higher energies than that in the T_1 state. This suggests the possibility of the different decay mechanism of *p*-**1** in the T_1 state from the case of *d*-**1** (usual lifetime of 9.7 ns), exhibiting the non-radiative decay through the thermally populated ^{3}MC state. The possible mechanism is direct relaxation of the T_1 to S_0 states according to the energy-gap law: the decay rate decreases exponentially with increasing the energy gap between excited and ground states [46–48]. Considering almost the same geometries of *p*-**1** between the S_0 and T_1 states, the law can be applied as the weak coupling limit. The lower energy band gap of 101 kJ mol^{-1} between the S_0 and T_1 states for *p*-**1** could explain the short lifetime, at least qualitatively, based on the energy gap law. The direct relaxation mechanism is consistent with the non-thermal decay process suggested by the very quick decay (unusual lifetime of 6.4 ps) for *p*-**1** in the T_1 state. The direct relaxation

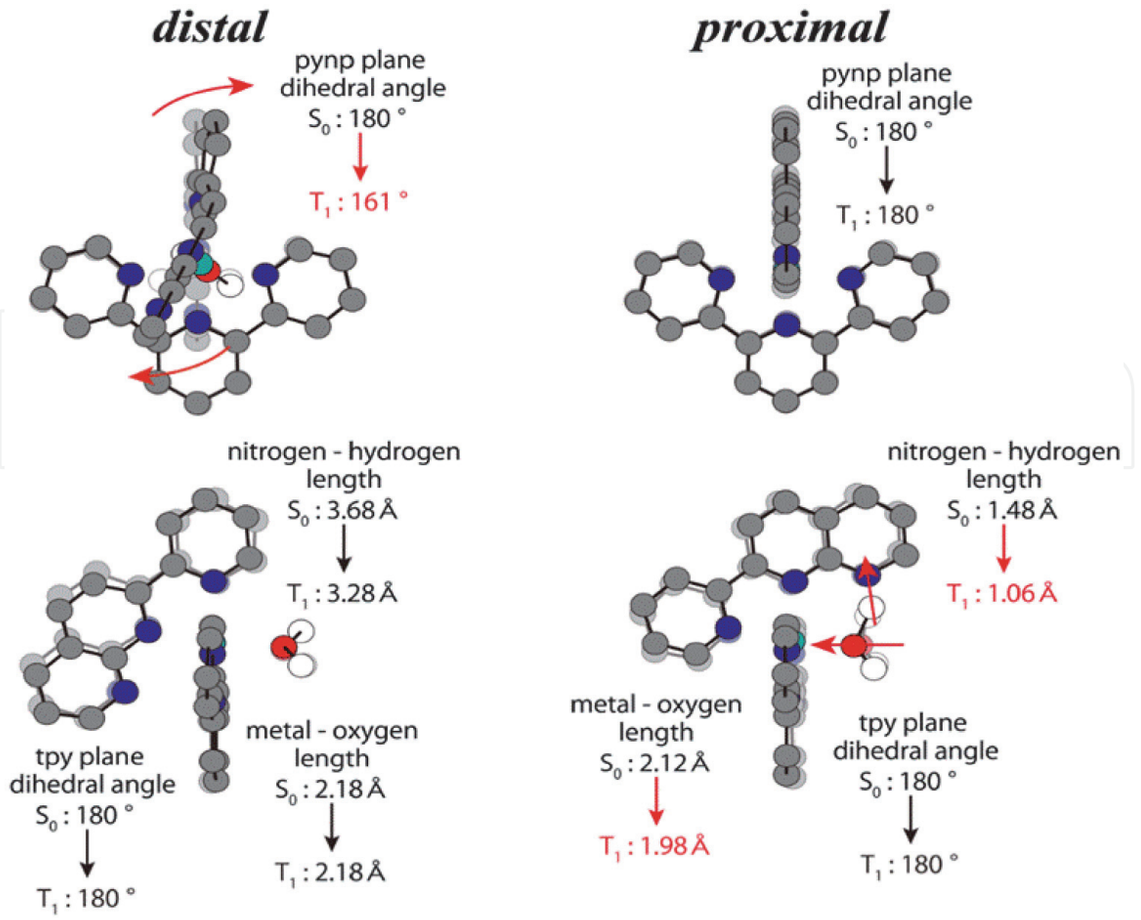

Figure 3.
Overlay of optimized structures of d-**1** *and* p-**1** *in the S_0 (lighter color) and T_1 (deeper color) states. The top and bottom structures are illustrated from the horizontal directions of the pynp and tpy planes, respectively. The colored labels of atoms are as follows: Green, Ru; gray, carbon; red, oxygen; blue, nitrogen; white, hydrogen. (reprinted with permission from ref. [36] copyright 2015 Elsevier).*

process from the T_1 states to the S_0 state (not *via* the ^{3}MC state) could explain the inert photoisomerization of *p*-**1**.

2.2 Reversible photoisomerization between *distal*- and *proximal*-[Ru(tpy)(pyqu)OH_2]$^{2+}$ isomers

The photoisomerization between *d*-**2** and *p*-**2** was examined to reveal the influence of structures of bidentate ligands on the photoisomerization of *d*-**1** (**Figure 5**) [34]. On irradiation of visible light to a D_2O solution of *p*-**2**, the 8.9 ppm peak characteristic of *p*-**2** in the ^{1}H NMR spectrum (**Figure 6A**) decreased with increasing the 9.5 ppm peak assigned to the *d*-**2** isomer. The ^{1}H NMR spectral change reached saturation in 5 min, while the 8.9 ppm peak did not completely disappear. This result suggests that the photoisomerization of *p*-**2** to *d*-**2** reaches a photostationary state (**Figure 5**). This shows that irreversible photoisomerization alters to reversible one by the replacement of the pynp ligand to pyqu in mononuclear Ru aquo complexes [21, 22]. From the integrated peak areas at 8.9 and 9.5 ppm, the equilibrated concentration ratio of *p*-**2**:*d*-**2** was calculated to be 76:24 (**Figure 6B**). The kinetic profiles of the photoisomerization of *p*-**2** to *d*-**2** were well fitted with a reversible reaction model, giving the observed rate constants of the forward reaction (*proximal* to *distal*, $(k_{p\text{-}d})_{obs}/s^{-1}$) of $4.3 \pm 0.1 \times 10^{-3}$ s^{-1} and the back reaction (*distal* to *proximal*, $(k_{d\text{-}p})_{obs}/s^{-1}$) of $1.2 \pm 0.03 \times 10^{-2}$ s^{-1} under the conditions employed ($\lambda > 420$ nm, 180 mW cm^{-2}), respectively (**Table 1**) [34]. The observed equilibrium constant were given to K_{obs} ($= (k_{p\text{-}d})_{obs}/(k_{d\text{-}p})_{obs}$) $= 0.34 \pm 0.01$ under

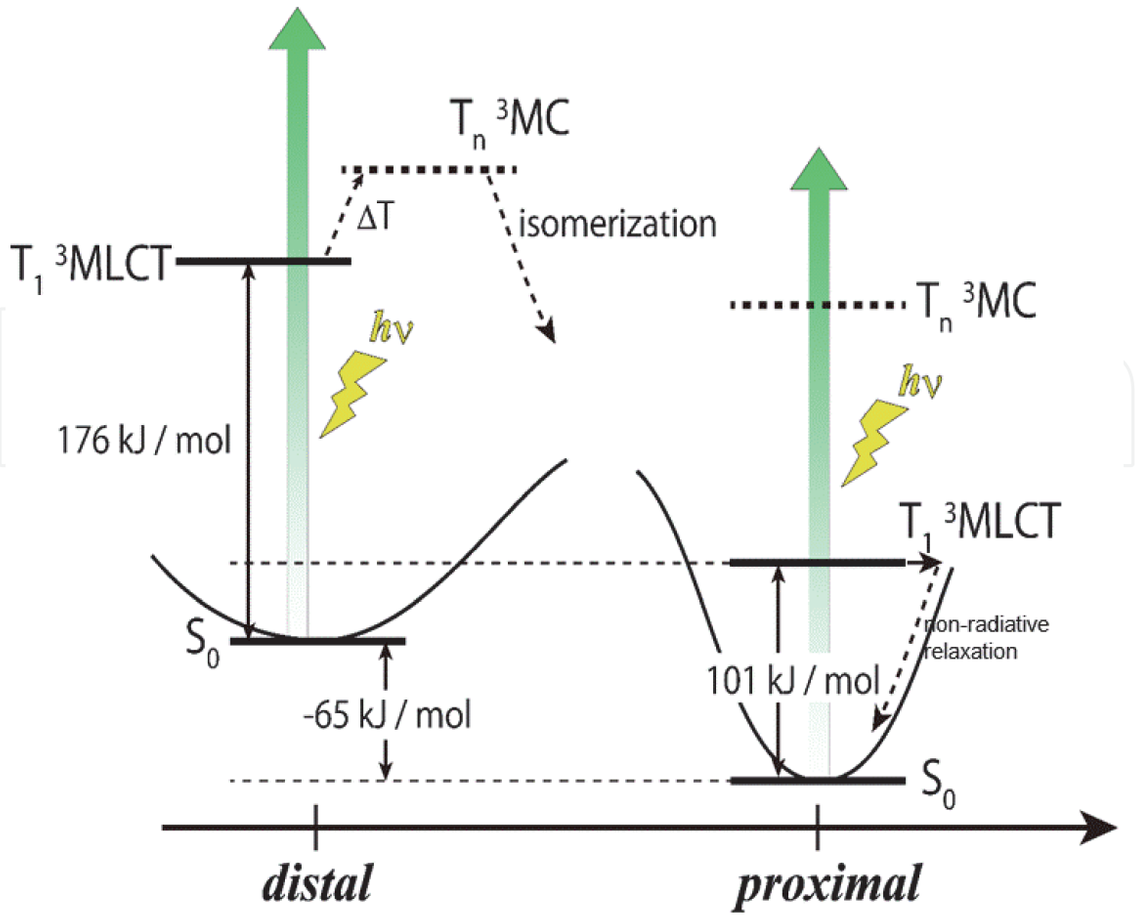

Figure 4.
DFT-calculated energy diagram of d-**1** *and* p-**1** *in the S_o and T_1 states. The speculated energy levels of T_n ^{3}MC states were described. (see text) (reprinted with permission from ref. [36] copyright 2015 Elsevier).*

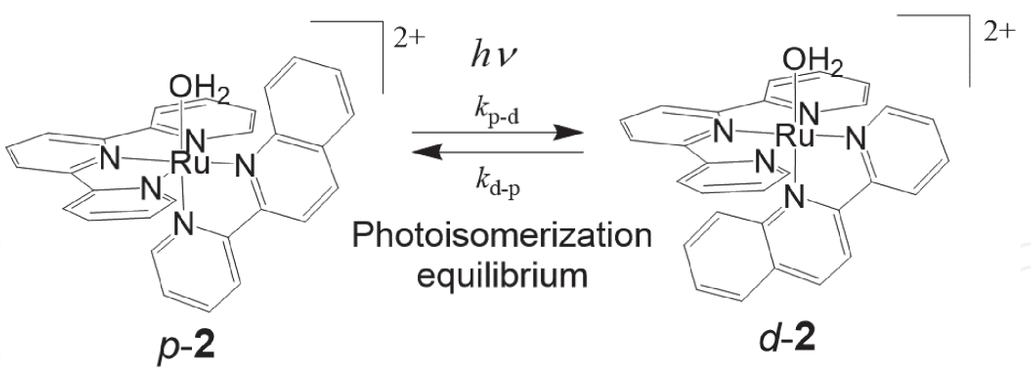

Figure 5.
Photoisomerization equilibrium between proximal- *and* distal-*[Ru(tpy)(pyqu)OH_2]$^{2+}$* (p-**2** *and* d-**2**) *isomers.*

the employed conditions. Both $(k_{p\text{-}d})_{obs}$ and $(k_{d\text{-}p})_{obs}$ increased linearly with respect to light intensity up to 180 mW cm^{-2}, suggesting that the photoexcited states of *p*-**2** and *d*-**2** isomers are also involved in the forward and back reactions, respectively [34]. As shown in **Figure 7**, $(k_{p\text{-}d})_{obs}$ and $(k_{d\text{-}p})_{obs}$ decreased from pD = 8 to 12, and the photoisomerization did not take place at all above pD =12 [34]. This result implies that both hydroxo isomers, *proximal*- and *distal*-[Ru(tpy)(pyqu)OD]$^+$ are inert for the forward and back photoisomerization reactions, respectively, as observed in the case of *distal*-[Ru(tpy)(pynp)OH]$^+$ [21, 22]. The pD-dependent $(k_{p\text{-}d})_{obs}$ and $(k_{d\text{-}p})_{obs}$ analysis demonstrated inflection points at pD = 10.5 and 9.8 for the forward

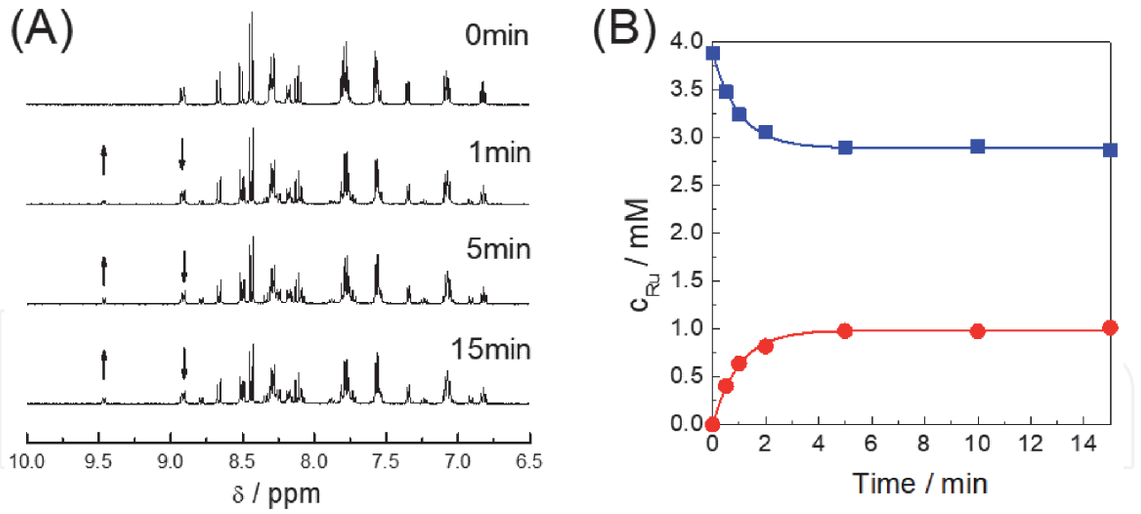

Figure 6.
(A) Time course of ^{1}H NMR spectral changes during the photoisomerization of p-**2** *(3.9 mM, pD = 8.4) with 180 mW/cm² visiblelight irradiation (λ > 420 nm) in D_2O. (B) Kinetic profiles of* p-**2** *(blue square) and* d-**2** *(red circles). (reproduced from ref. [34] with permission of John Wiley & Sons, Inc.).*

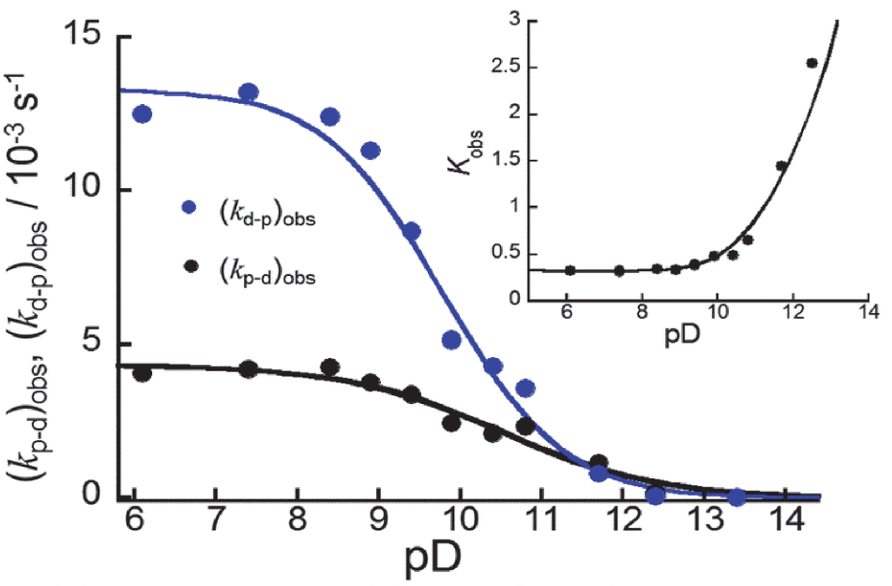

Figure 7.
Plots of observed rate constants ($(k_{p\text{-}d})_{obs}$ and $(k_{d\text{-}p})_{obs}$) vs. pD for the photoisomerization reactions shown in ***Figure 5****. Visible light (λ > 420 nm, 180 mW/cm²) was irradiated to the* p-**2** *(3.9 mM) in D_2O at 25°C. Inset shows diagram of observed equilibrium constants K_{obs} vs. pD. (reproduced from ref. [34] with permission of John Wiley & Sons, Inc.).*

and back reactions, respectively. These values are close to the pK_a of *p*-**2** (pK_a = 10.5) and *d*-**2** (pK_a = 9.4) (**Table 1**). The difference in pK_a values (1.1) between *p*-**2** and *d*-**2** results in the markedly pD-dependent K_{obs} values (inset of **Figure 7**). K_{obs} increased above pH = 9, and reached its maximum value (K_{obs} = 2.5) at pH = 12. This trend is consistent with the observation that the yield of *d*-**2** generated in the photoisomerization raised from 26–65% on increasing from pH 5.7 to 12.

The thermal dependent kinetics for $(k_{p\text{-}d})_{obs}$ and $(k_{d\text{-}p})_{obs}$ in a temperature range of 25 to 70°C gives E_a = 30.6 ± 2.9 and 23.3 ± 2.1 kJ mol^{-1} for the forward and back reactions, respectively. The higher E_a of the forward reaction ($(k_{p\text{-}d})_{obs}$) compared to the back one ($(k_{d\text{-}p})_{obs}$) is attributable to the unfavorable loss of the hydrogen bond (C-H···O) between the H atom bonded to 8-C of the quinoline moiety of the pyqu ligand and the O atom of the aquo ligand upon water

dissociation for photoisomerization. The van't Hoff plots for K_{obs} gave $\Delta H = 7.7 \pm 2.7$ kJ mol^{-1}, that is close to enthalpy for the hydrogen bond (5.4 kJ mol^{-1}) of C-H···O in the benzene-water complex [49].

The Φ values for the forward and back photoisomerization reactions were estimated to be 0.34% and 1.1% from the experiments using monochromatic light (520 nm, 26.4 mW cm^{-2}) (**Table 1**). The higher Φ (1.1%) of *d*-**2** compared to that (0.34%) of *p*-**2** could be attributed to the enthalpy of hydrogen bond (C-H···O) of *p*-**2** (decreased Φ for *p*-**2**) and the steric repulsion between the H atom bonded to 8-C of the quinoline moiety of pyqu and the tpy plane for *d*-**2** (increased Φ for *d*-**2**). The Φ value of 1.1% for photoisomerization from *d*-**2** to *p*-**2** is 3.5 times higher than that (0.31%) for the photoisomerization from *d*-**1** to *p*-**1** under the same concentration [34]. This could also be ascribed to the dominant steric repulsion between the tpy ligand and the H atom bonded to 8-C of the quinoline ring of pyqu for *d*-**2**, compared to the repulsion between the tpy ligand and the uncoordinated nitrogen of the naphthyridine ring of pynp for *d*-**1**.

2.3 New synthetic strategy for dinuclear ruthenium(II) complexes utilizing the photoisomerization

The photoisomerization of Ru(II) aqua complexes was applied to the strategic synthesis of dinuclear Ru complexes that are difficult to be synthesized by conventional thermal reactions so far. Herein, we succeeded to newly synthesize several dinuclear Ru(II) complexes, *proximal*, *proximal*-$[Ru_2(tpy)_2LXY]^{3+}$ (L = 5-phenyl-2,8-di(2-pyridyl)-1,9,10- anthyridine, X and Y = other coordination sites; denoted as *p*,*p*-**Ru_2XY**) utilizing the photoisomerization of a mononuclear Ru aquo complex [37]. The tetradentate backbone ligand L was used to form a *proximal*, *proximal* - dinuclear Ru(II) structure (**Figure 8**). The reaction of $[Ru(tpy)Cl_3]$ with L gave *distal*-$[Ru(tpy)LCl]^+$ (*d*-**3Cl**) selectively in ethanol in a 59% isolated yield. This selective formation of *d*-**3Cl** was possibly caused by the steric hindrance of L with a chloro ligand. *d*-**3Cl** was then converted to *distal*-$[Ru(tpy)LOH_2]^{2+}$ (*d*-**3**) by chloro subtraction with a silver salt in water in a 90% isolated yield. The thermal reaction of *d*-**3** with a second ruthenium center $[Ru(tpy)Cl_3]$ for dimerization failed to give

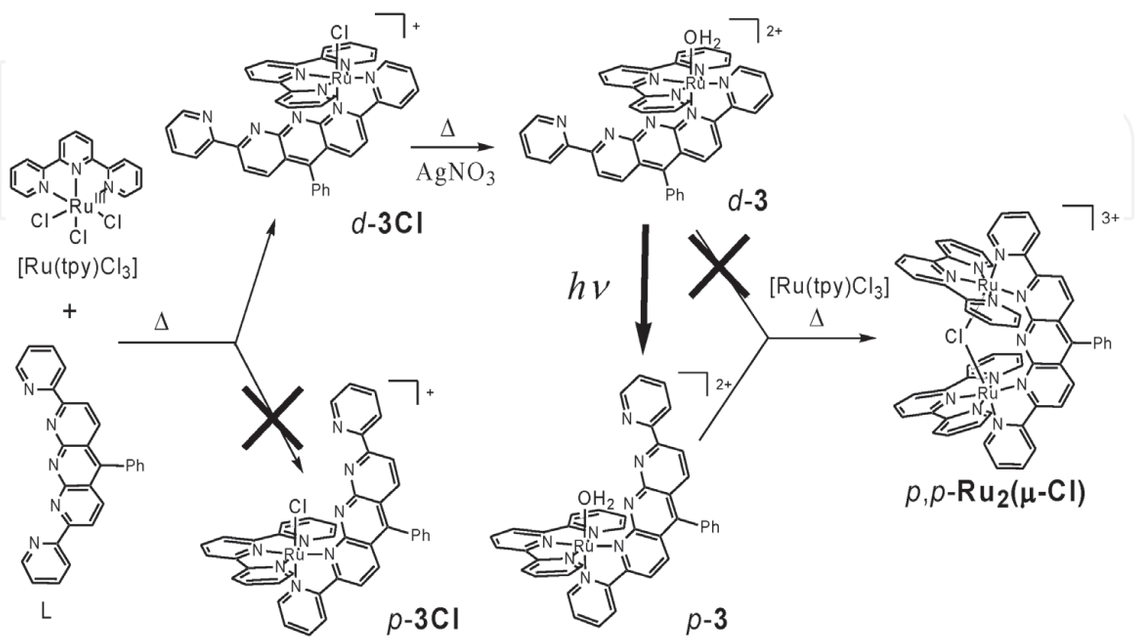

Figure 8.
Synthetic scheme of a μ-Cl bridged dinuclear ruthenium complex, p,p-***Ru_2(μ-Cl)*** *using photoisomerization of* d-*3. (reproduced from ref. [37] with permission of American Chemical Society).*

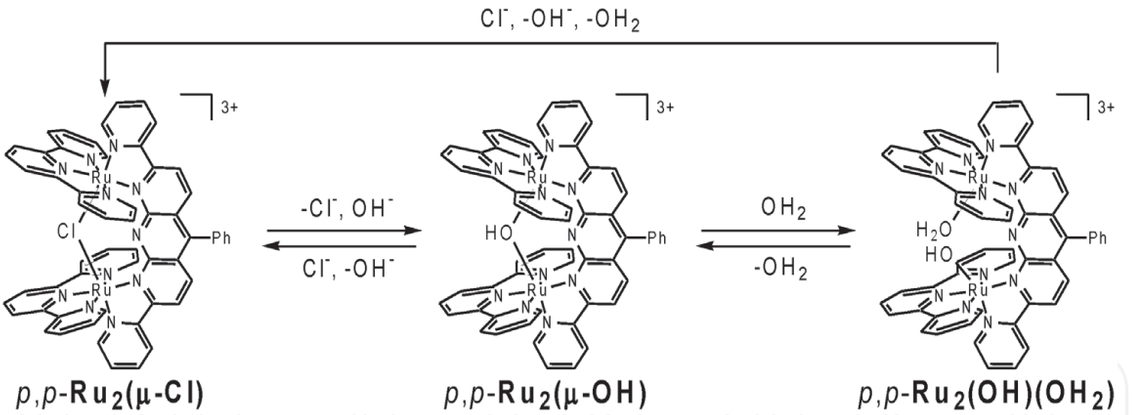

Figure 9.
Reversible bridging-ligand substitution reactions among p,p-***Ru₂(μ-Cl),*** p,p-***Ru₂(μ-OH)*** p,p-***Ru₂(OH)(OH₂).***

the *proximal*, *proximal*-dinuclear Ru(II) complex owing to the steric hindrance located between the tpy ligand on the *d*-**3** and the one on $[Ru(tpy)Cl_3]$. However, if the photoisomerization of *d*-**3** to *proximal*-$[Ru(tpy)LOH_2]^{2+}$ (*p*-**3**) is utilized (**Figure 8**), the steric constraint of *d*-**3** for formation of the *proximal*,*proximal*-dinuclear Ru(II) species could be avoided. The photoisomerization of *d*-**3** stoichiometrically progressed to form *p*-**3** in water/ethanol mixture under visible light irradiation ($\lambda > 420$ nm). The subsequent thermal reaction of *p*-**3** with $[Ru(tpy)Cl_3]$ in water/ethanol mixture successfully generated *proximal*,*proximal*-$[Ru_2(tpy)_2L(\mu\text{-}Cl)]^{3+}$ (*p*,*p*-**Ru_2(μ-Cl)** in a 67% isolated yield that was unambiguously characterized by X-ray diffraction [37]. The *p*,*p*-**Ru_2(μ-Cl)** was converted to the *proximal*,*proximal*-$[Ru_2(tpy)_2L(\mu\text{-}OH)]^{3+}$ (*p*,*p*-**Ru_2(μ-OH)**) in neutral or slightly basic aqueous medium via substitution of the μ-Cl bridge with an OH^- ion as shown in **Figure 9** [37, 38]. The *p*,*p*-**Ru_2(μ-OH)** was then converted to *proximal*,*proximal*-$[Ru_2(tpy)_2L(OH)(OH_2)]^{3+}$ (*p*,*p*-**Ru_2(OH)(OH_2)**) via insertion of a water molecule to the central core to reach equilibrium between *p*,*p*-**Ru_2(μ-OH)** (~10%) and *p*,*p*-**Ru_2(OH)(OH_2)**.

3. Water oxidation catalysis by ruthenium(II) aquo complexes

The mononuclear ruthenium polypyridyl aquo complexes are promising WOCs to understand water oxidation chemistry and provide the guided thought for efficient WOCs because of their simple structures, high catalytic activities, ease of chemical modification, and informative knowledge including catalytic mechanisms [13, 21–23, 34, 35, 40, 50–52]. Controlling the electron density on the metal center as an active site by alternating the substituent groups on their ligands is a common approach to reveal the mechanism and influencing factors for water oxidation catalysis.

The molecular WOCs take part in the process of the four electrons and four protons removal from two water molecules, either consecutively or concerted, to form the O-O bond. Understanding the mechanism of the O-O bond formation is vital in improvement of molecular WOCs. Two main classes of proposed reaction mechanisms at metal centers are shown in **Figure 10**; water nucleophilic attack (*WNA*) on metal-oxo centers (M = O) and interaction of two M-O centers (*I2M*) [53–56]. In the *WNA* mechanism (**Figure 10a**), an electrophilic high-valent metal-oxo (M^{n+} = O) species is formed via multiple consecutive oxidation steps. A nucleophilic attack of a water molecule on the M^{n+} = O species occurs, that leads to formation of a hydroperoxide ($M^{(n-2)+}$-OOH) species. Further oxidation and

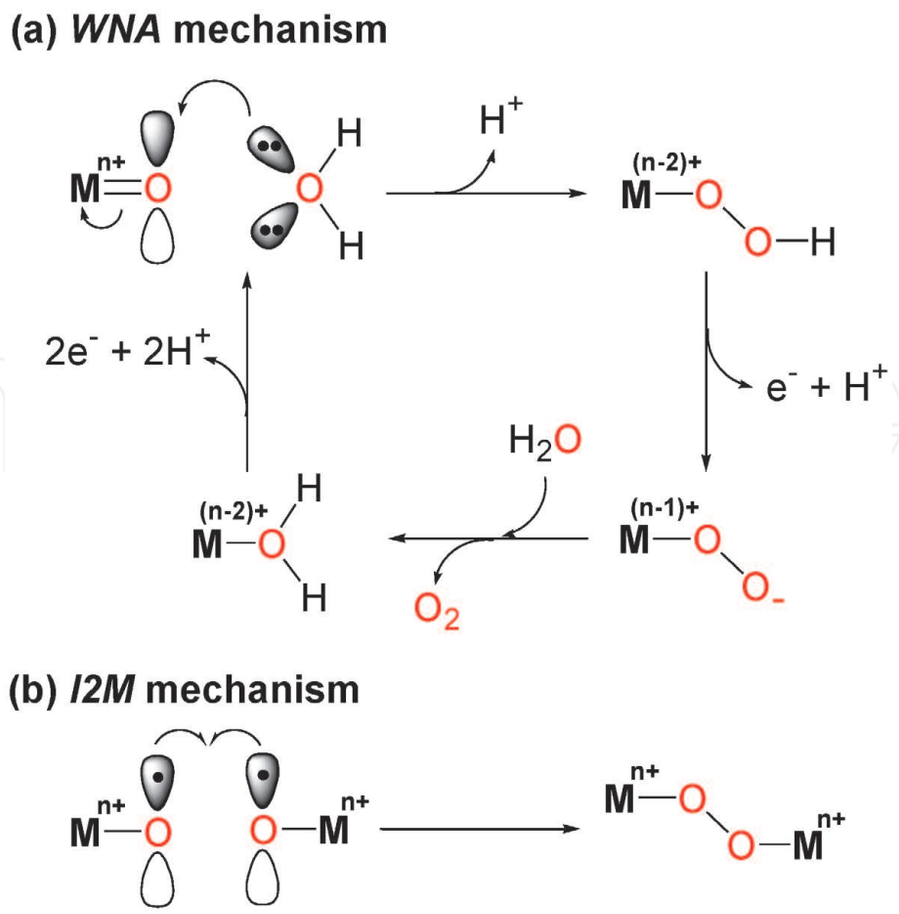

Figure 10.
Schematic representation of the two mechanistic pathways for O-O bond formation. (reproduced with permission from ref. [20]. Copyright 2019 Wiley).

deprotonation steps generate a $M^{(n-1)+}$-OO^{-} intermediate, which releases O_2 and converts to $M^{(n-2)+}$-OH_2 with incorporation of OH_2. A lot of mononuclear complexes have been proposed to undergo the *WNA* mechanism for water oxidation [21–23, 34, 35, 40, 51, 52, 57, 58]. In the *I2M* mechanism (**Figure 10b**), the coupling of either two M^{n+}-O oxyl radicals or coupling of one M^{n+}-O oxyl radical with another M^{n+}-O unit of a non-radical character affords a peroxo M^{n+}-O-O-M^{n+} intermediate, which releases O_2 and returns to 2 $M^{(n-2)+}$-OH_2 with incorporation of OH_2. It involves intramolecular [37, 59, 60] and intermolecular [61, 62] pathways.

In this section, we introduce our recent progress on chemical and electrochemical water oxidation catalyses by mono- and dinuclear ruthenium(II) aquo complexes in homogeneous systems. Firstly, substitution effects on the catalytic activity and mechanism of mononuclear ruthenium(II) aquo complexes for chemical water oxidation are described in Section 3-1. Secondly, the difference in the catalytic properties between *distal*−/*proximal*-isomers is explicated in Section 3-2. Finally, the electrocatalytic activities of a series of dinuclear ruthenium(II) complexes are discussed in Section 3-3.

3.1 Substitution effect on the catalytic activities of mononuclear ruthenium complexes for water oxidation

To investigate the catalytic aspects of $[Ru(Rtpy)(bpy)(H_2O)]^{2+}$ (Rtpy = 2,2′:6′,2″-terpyridine derivatives) complexes (**4R**) having a variety of 4′-substituent groups on Rtpy ligand (**Figure 11**), chemical water oxidation experiments were performed in a homogeneous aqueous solution using a Ce^{IV} as a

sacrificial oxidant [39, 40]. For **4EtO** (R = EtO), O_2 was significantly evolved from the catalytic solution, and the amount (n_{O2}/μmol) of O_2 evolved increased linearly until 100 min and then saturated to 35 μmol at 4 h, which is 5 times higher than that for **4H** (**Figure 12**) [39]. The initial O_2 evolution rates (v_{O2}/mol s^{-1}) were calculated from the initial slopes. The v_{O2} for **4EtO** increased with the Ce^{IV} concentration (c_{Ce}/M) and reached a saturation at c_{Ce} = 1.0 M (**Figure 13**), indicating that O_2 evolution is zero order with respect to Ce^{IV} under the large excess Ce^{IV} conditions. This behavior was well-analyzed by Michaelis–Menten-like kinetics to give the maximum catalytic rate (v_{max}) of 1.5 (±0.08) x 10^{-1} mol s^{-1} (**4EtO** mol)$^{-1}$ and the constant (K_m = 1.2 (±0.06) mmol) in terms of the Ce^{IV} concentration for the half value of v_{max}. The oxidation reaction from Ru^{IV}=O to Ru^{V}=O by Ce^{IV} could involve the redox equilibrium prior to oxygen evolution because the redox potential (1.45 V vs. SCE) of Ru^{IV}=O/Ru^{V}=O for **4EtO** is close to standard potential (E° = 1.47 V vs. SCE (1.71 V vs. NHE) [63]) of $Ce^{III/IV}$. The redox equilibrium presumably leads to saturation of the v_{O2} with increase of the Ce^{IV} concentration (**Figure 13**). The v_{O2} increased linearly with the **4EtO** concentration (c_{Ru}/M) under the large excess Ce^{IV} conditions (c_{Ce} = 0.1 M, c_{Ru} = ~ 0.2 mM, 5.0 ml water) (**Figure 14**), showing that the O_2 evolution is a first order process with respect to **4EtO**. This result is consistent with the case of earlier-reported mononuclear Ru(II) aquo complexes [50, 51].

The mechanism of water oxidation by **4R** is shown in **Figure 15** based on the WNA mechanism [50, 51, 56]. **4R** (abbreviated to Ru^{II}-OH_2 as the oxidation state) is oxidized by Ce^{IV} to Ru^{III}-OH_2 by a 1-electron process, and subsequently oxidized to Ru^{IV}=O by two-proton/one-electron process at pH = 1.0 [39, 40]. Ru^{IV}=O is further oxidized to Ru^{V}=O, involving the above-mentioned redox equilibrium (step I, **Figure 15**). Ru^{V}=O undergoes water nucleophilic attack (step II, **Figure 15**) to

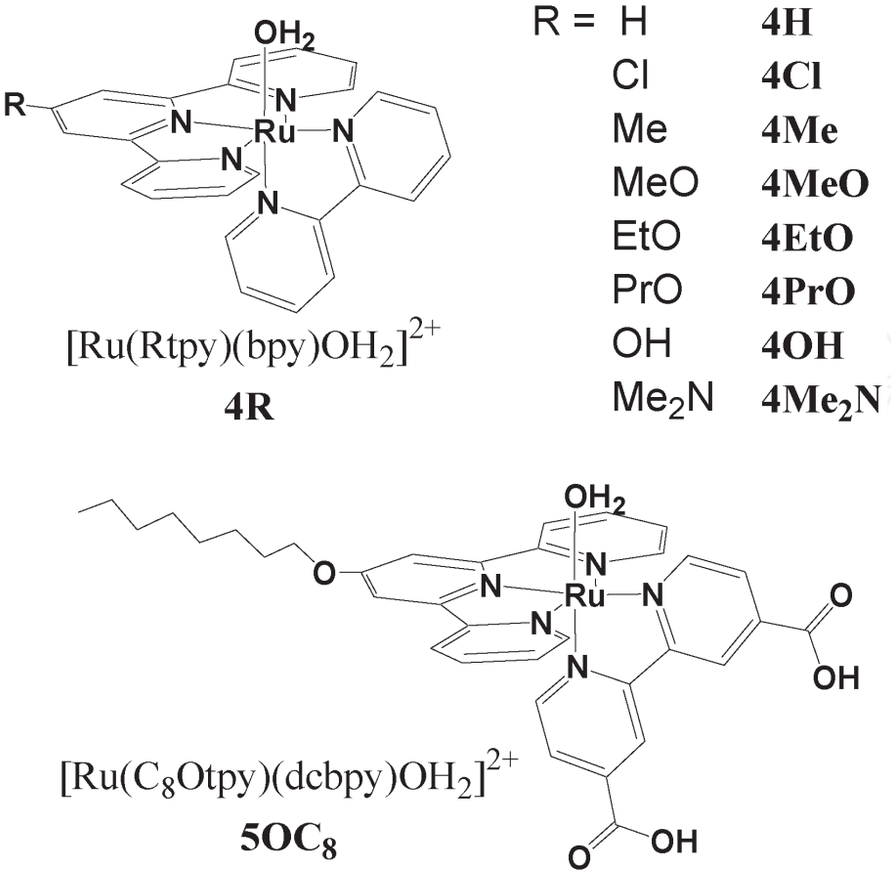

Figure 11.
Chemical structures of mononuclear ruthenium(II) aquo complexes.

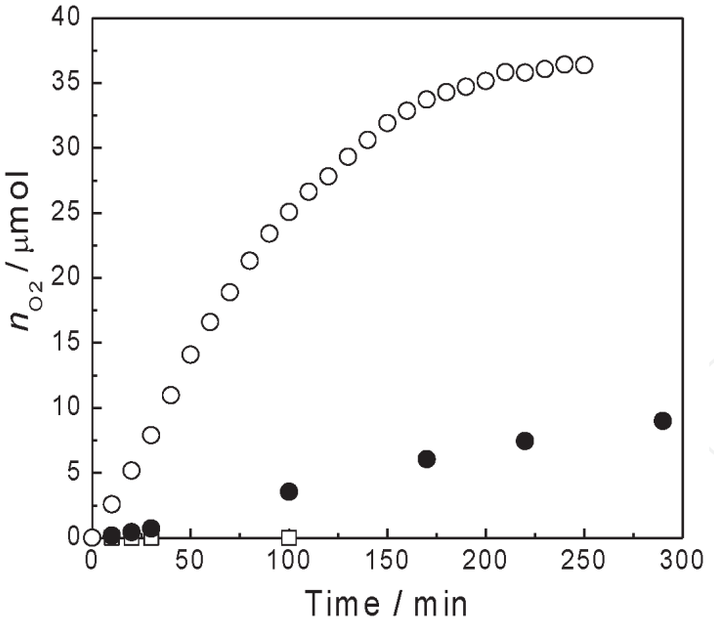

Figure 12.
*Time courses of the amount (n_{O2}/Mol) of O_2 evolved in chemical water oxidation experiments in an aqueous solution at 25°C using a Ce^{IV} oxidant. c_{Ce} = 0.1 M (0.5 mmol); complexes, 20 μM (0.1 μmol); pH = 1.0; liquid volume, 5.0 ml. (○) **4EtO**, (●) **4H** and (□) without complex. (reproduced with permission from ref. [39]. Copyright 2011 the Royal Society of Chemistry).*

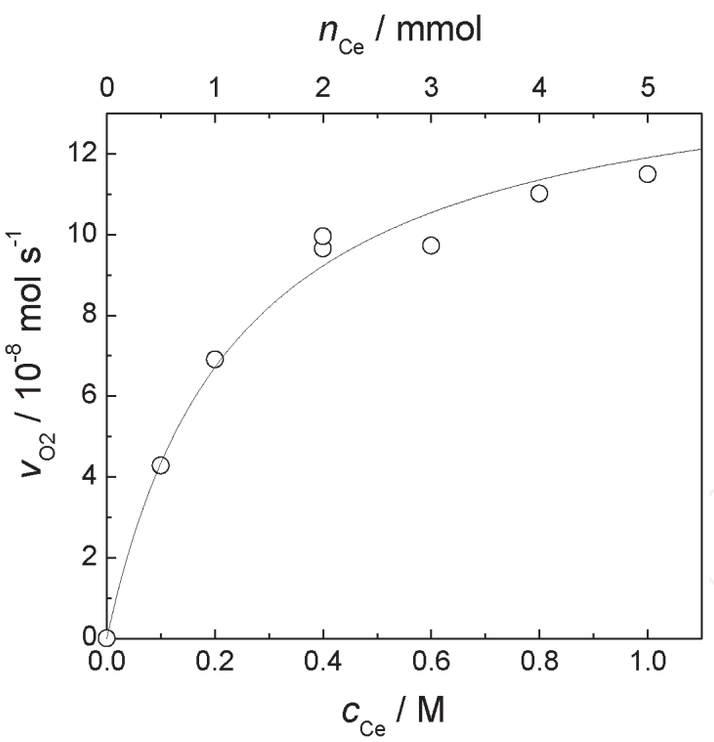

Figure 13.
*Plots of v_{O2} versus the Ce^{IV} concentration (c_{Ce}/M) in chemical water oxidation experiments using 0.2 mM **4EtO** (5.0 ml water) at 25°C. the solid line is the simulated curve based on a Michaelis–Menten-like kinetic equation. (reproduced with permission from ref. [39]. Copyright 2011 the Royal Society of Chemistry).*

form an O-O bond in the Ru^{III}-OOH intermediate. Finally, O_2 is produced via further oxidation to Ru^{IV}-OO^{-}, with Ru^{II}-OH_2 regenerated by incorporation of water.

The v_{O2} showed a first-order dependence on the complex amount for all the **4R** derivatives (**Figure 14**) [40], suggesting that O_2 is produced by a unimolecular

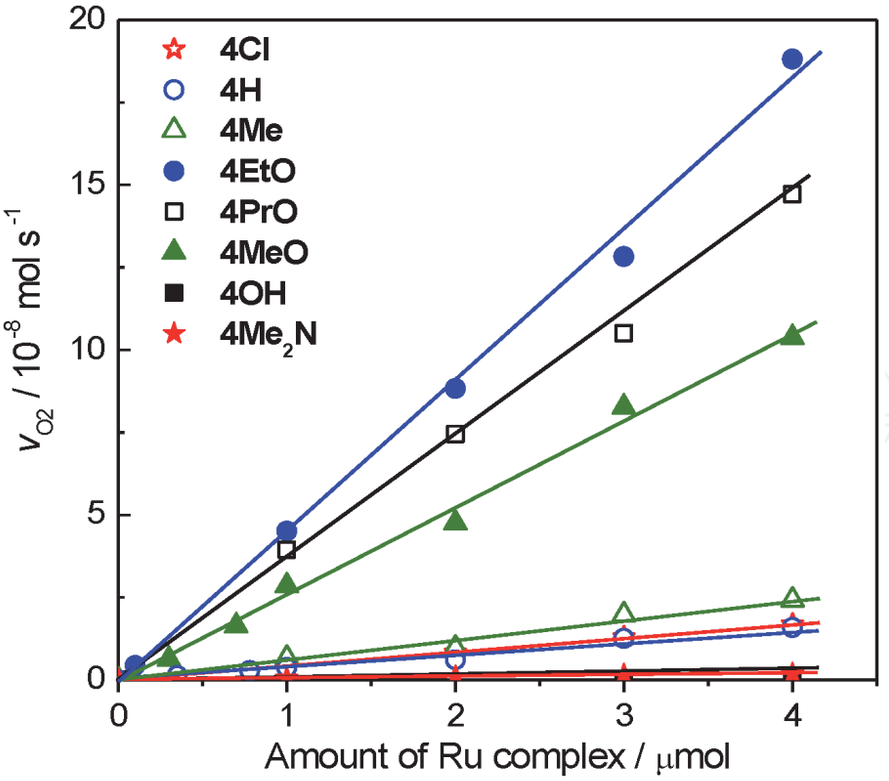

Figure 14.
*Plots of initial O_2 evolution rate (v_{O_2}/Mol s^{-1}) versus the amount of **4R** complexes. c_{Ce} = 0.1 M, 5.0 ml water, pH = 1.0. (reproduced with permission from ref. [40]. Copyright 2019 American Chemical Society).*

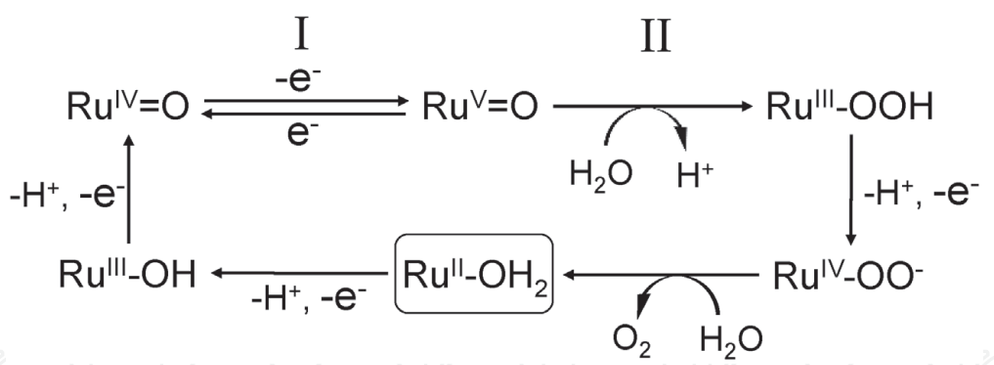

Figure 15.
*Mechanism of water oxidation by **4R** complexes at pH = 1.0. (reprinted with permission from ref. [40]. Copyright 2019 American Chemical Society).*

reaction of **4R**. Turnover frequencies (k_{O2}/s^{-1}) were calculated from the slopes of the linear relationships. The k_{O2} values were largely affected by the Rtpy ligands, being variable from 0.05 to 44 x 10^{-2} s^{-1} (as the highest k_{O2} for **4EtO**) by a factor of 880 (**Table 2**). The k_{O2} values were plotted with respect to Hammett constant σ_p of the 4′-substituents of Rtpy ligands in **Figure 16A**. However, the Me_2N group is protonated to give Me_2NH^+ under the catalytic conditions (pH = 1.0), and the σ_p value of Me_2NH^+ was assumed as σ_p = 0.71 of the midpoint between σ_p = 0.60 for protonated amino group and σ_p = 0.82 for protonated trimethylamino group [64]. The k_{O2} values were almost constant (3.4 ~ 6.1 x 10^{-2} s^{-1}) in a range of σ_p = −0.17 (R = Me) ~ 0.23 (R = Cl), although the k_{O2} value (5 x 10^{-4} s^{-1}) of **4Me$_2$N** is lower than these values. The k_{O2} value increased sharply at σ_p = −0.24 (R = EtO) to 4.4 x10^{-1} s^{-1} as the maximum, and thereafter decreased with the σ_p decrease to −0.37 (R = OH). This result demonstrates that very critical Hammett constant

Complexes	Abbreviation	$k_{O2}/10^{-3}$ s^{-1}	Ref
$[Ru(tpy)(bpy)OH_2]^{2+}$	**4H**	34	[39]
$[Ru(Cltpy)(bpy)OH_2]^{2+}$	**4Cl**	43	[40]
$[Ru(Metpy)(bpy)OH_2]^{2+}$	**4Me**	61	[40]
$[Ru(MeOtpy)(bpy)OH_2]^{2+}$	**4MeO**	240	[40]
$[Ru(EtOtpy)(bpy)OH_2]^{2+}$	**4EtO**	440	[40]
$[Ru(PrOtpy)(bpy)OH_2]^{2+}$	**4PrO**	331	[40]
$[Ru(OHtpy)(bpy)OH_2]^{2+}$	**4OH**	0.9	[40]
$[Ru(Me_2Ntpy)(bpy)OH_2]^{2+}$	**4Me$_2$N**	0.5	[40]
distal-$[Ru(tpy)(pynp)OH_2]^{2+}$	*d*-**1**	3.8	[21]
proximal-$[Ru(tpy)(pynp)OH_2]^{2+}$	*p*-**1**	0.48	[21]
distal-$[Ru(Cltpy)(pynp)OH_2]^{2+}$	*d*-**1Cl**	6.3	[35]
proximal-$[Ru(Cltpy)(pynp)OH_2]^{2+}$	*p*-**1Cl**	0.39	[35]
distal-$[Ru(tpy)(pyqu)OH_2]^{2+}$	*d*-**2**	1.0	[34]
proximal-$[Ru(tpy)(pyqu)OH_2]^{2+}$	*p*-**2**	1.7	[34]

Table 2.
Summary of k_{O2} *by mononuclear Ru(II) aquo complexes.*

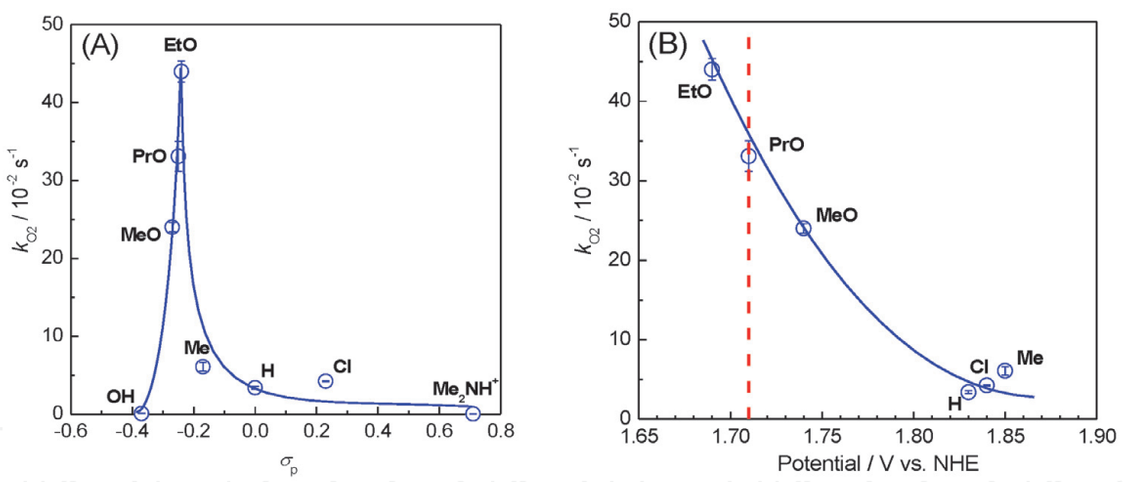

Figure 16.
Plots of the turnover frequency (k_{O2}/s^{-1}) versus *Hammett constant* (σ_p) *of 4′-substituent groups (A) and* versus *the redox potentials of a* Ru^{IV}=O/Ru^{V}=O *pair (B). The* Me_2N *group is protonated to a* Me_2NH^+ *group under the experimental conditions for water oxidation (pH = 1.0), and the* σ_p *value of* Me_2NH^+ *was assumed as* σ_p *= 0.71 of the midpoint between* σ_p *= 0.60 for protonated amino group and* σ_p *= 0.82 for protonated trimethylamino group [64]. The redox potentials were estimated from* E_{ap} *values, where* E_{ap} *is an anodic peak potential corresponding to the* Ru^{IV}=O/Ru^{V}=O *couple in a cyclic voltammogram for each of* ***4R*** *complexes. The red dashed line indicates the standard redox potential of* $Ce^{III/IV}$ *[63]. (Reproduced with permission from ref. [40]. Copyright 2019 American Chemical Society).*

($\sigma_p = -0.27 \sim -0.24$) exists for the high k_{O2} values. The very low k_{O2} values for **4OH** and **4Me$_2$N** arise from the difficulty of Ru^{V}=O formation. Most likely, **4OH** and **4Me$_2$N** are considered to decompose through their ligand oxidation during water oxidation catalysis, as reported recently [65, 66].

The k_{O2} values were plotted with respect to redox potentials of Ru^{IV}=O/Ru^{V}=O in **Figure 16B**. The k_{O2} values increased with the decrease of the redox potentials in an order of **4H**, **4Cl**, **4Me** < **4MeO** < **4PrO** < **4EtO**. This indicates that the potential for formation of Ru^{V}=O species is essential in the water oxidation catalysis under the employed conditions. This k_{O2} profile can be explained by the increased

fraction of Ru^{V}=O in the equilibrium. In this case, the oxidation rate (step I in **Figure 15**) from Ru^{IV}=O to Ru^{V}=O by Ce^{IV} could be comparable with the rate of the nucleophilic attack of water on Ru^{V}=O (step II in **Figure 15**) to be involved in a rate-determining step. The O-O bond formation process *via* water nucleophilic attack could be no longer a rate-determining step singularly. One might deservedly expect that the k_{O2} values of **4H**, **4Cl**, and **4Me** with the higher redox potentials of Ru^{IV}=O/Ru^{V}=O are higher than those of **4MeO**, **4PrO** and **4EtO** with the lower redox potentials since water nucleophilic attack on Ru^{V}=O (step II, **Figure 15**) is assumed to accelerate because of the higher electrophilicity of the oxo of Ru^{V}=O for the formers. By contrast, the k_{O2} values of **4H**, **4Cl**, and **4Me** were indeed lower than those of **4MeO**, **4PrO** and **4EtO**, which could be explained by the slow oxidation rate (step I in **Figure 15**) from Ru^{IV}=O to Ru^{V}=O involved in a rate-determining step.

3.2 Comparison in catalytic activities between *distal* and *proximal* isomers of mononuclear ruthenium complexes

To explore the catalytic aspects of a series of *distal* and *proximal* isomers for the mononuclear Ru(II) aquo complexes, chemical water oxidation experiments were conducted in a homogeneous aqueous solution using a Ce^{IV} oxidant [21, 22]. O_2 was significantly evolved from a mixed solution of *d*-**1** and Ce^{IV}, and n_{O2} increased linearly with time until 50 min (**Figure 17**). v_{O2} increased linearly with respect to the amount of the complex, and the slope of the linear relationship provides k_{O2} = 3.8 x 10^{-3} s^{-1} (**Figure 18**). The same chemical water oxidation experiments were carried out after visible light irradiation to the solution of *d*-**1** for 1 h to generate *p*-**1** completely (**Figure 1**). n_{O2} dramatically decreased compared with the case before light irradiation (**Figure 17**). The linear plot of v_{O2} with the catalyst

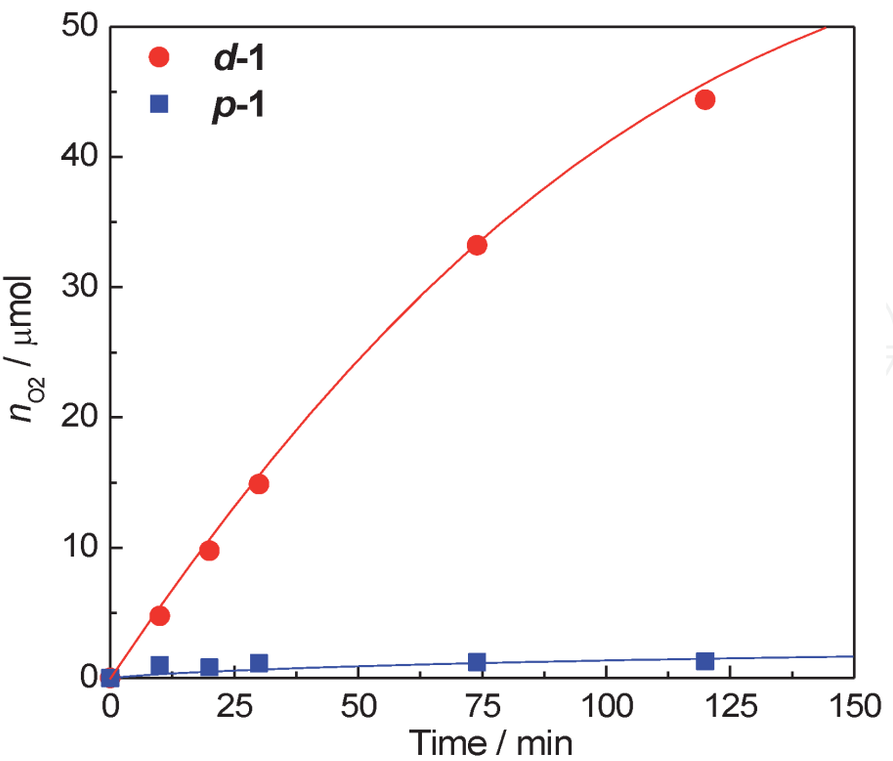

Figure 17.
*Time courses of the amount (n_{O2}/μmol) of O_2 evolved in chemical water oxidation experiments in an aqueous solution at 25°C using a Ce^{IV} as a sacrificial oxidant. c_{Ce} = 0.1 M (0.5 mmol); Ru complex, 1.0 μmol; pH = 1.0; liquid volume, 5.0 ml. (●) d-**1**, (■) p-**1**. (Reproduced with permission from ref. [21]. Copyright 2011 American Chemical Society).*

amount provided k_{O2} = 4.8 x 10^{-4} s^{-1} for *p*-**1**, indicating that the observed k_{O2} value is decreased due to photoisomerization of *d*-**1** to *p*-**1** by nearly an order of magnitude. This result tells us that we have to pay attention to the observed catalytic activity decrease due to photoisomerization of *d*-**1** to *p*-**1** when *d*-**1** is applied to photocatalytic systems.

The chemical water oxidation catalyzed by *d*-**1Cl** and *p*-**1Cl** was investigated under the same conditions as the *d*−/*p*-**1** isomer system to understand the effect of 4′-chloro-substitusion on tpy ligand on the catalytic activity of the *distal*−/*proximal*-isomer complexes for water oxidation [35]. v_{O2} increased linearly with respect to the complex amount for *d*-**1Cl** and *p*-**1Cl**, as is the case of the *d*−/*p*-**1** isomer system (**Figure 18**). k_{O2} (6.3×10^{-3} s^{-1}) for *d*-**1Cl** was 15 times higher than that (3.9×10^{-4} s^{-1}) for *p*-**1Cl**. From a perspective of the effect of the chloro-substitution on tpy, k_{O2} for *d*-**1Cl** was also 1.6 times higher that (3.8×10^{-3} s^{-1}) for *d*-**1**, while k_{O2} for *p*-**1Cl** was 1.2 times lower than that (4.8×10^{-4} s^{-1}) for *p*-**1**. If assuming that the O-O bond formation *via* the nucleophilic attack of water on the Ru^{V}=O intermediate is the rate-determining step, k_{O2} could increase by the chloro substitution because electrophilicity of Ru^{V}=O increased, as is the case for *d*-**1Cl** relative to *d*-**1**. However, another explanation is needed for the k_{O2} decrease for *p*-**1Cl** relative to *p*-**1**. For instance, there are cases that the rate for oxidation of Ru^{IV}=O to Ru^{V}=O could be involved in a rate-determining step, or that the stabilities of the complexes are different, as pointed out in the Section 3-1.

The k_{O2} value (1.7×10^{-3} s^{-1}) of *p*-**2** was higher than that (1.0×10^{-3} s^{-1}) of *d*-**2** by a factor of 1.7 (**Table 2**) [34]. This result is in contrast to the *d*−/*p*-**1** and *d*−/*p*-**1Cl** isomer systems, in which k_{O2} of *distal*-isomers are higher than those of the *proximal*-ones by one order of magnitude. The k_{O2} value of *p*-**2** is 3.5 times higher

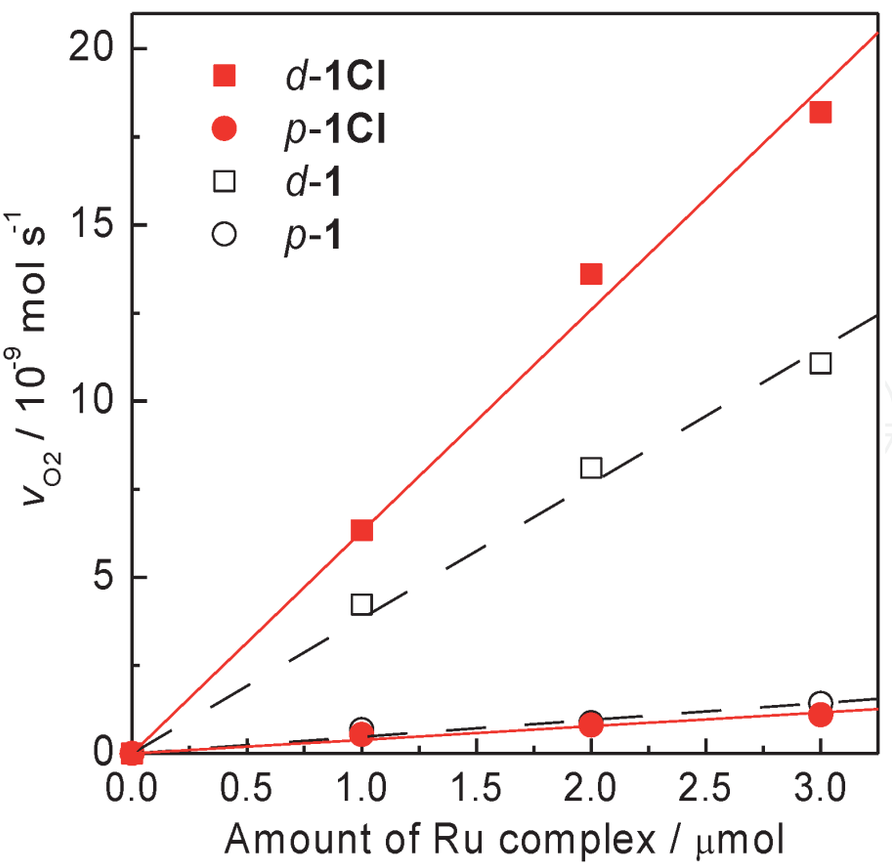

Figure 18.
Plots of initial rate (v_{O2} / mol s^{-1}) of O_2 evolved vs. the amount (μmol) of d-***1Cl*** (■), p-***1Cl*** (●), d-***1*** (□), p-***1*** (○). *Conditions:* c_{Ce} *= 0.1 M (0.5 mmol); liquid volume, 5.0 mL; pH = 1.0. (reproduced with permission from ref. [35]. Copyright 2015 Elsevier).*

than that (4.8×10^{-4} s^{-1}) of *p*-**1**, though the value of *d*-**2** is 3.8 times lower than that (3.8×10^{-3} s^{-1}) of *p*-**2** under the same conditions.

3.3 Electrocatalytic activities of a series of dinuclear ruthenium complexes for water oxidation

We investigated catalytic activities of *p*,*p*-**$Ru_2(OH)(OH_2)$** and the related mono- and dinuclear Ru(II) complexes (**Figures 8** and **9**) for electrochemical water oxidation in homogeneous solution [37]. The cyclic voltammogram (CV) of *p*,*p*-**$Ru_2(OH)(OH_2)$** displayed a higher anodic current after 1.2 V vs. SCE attributed to water oxidation (**Figure 19**). The catalytic current density increased to 3.5 mA cm^{-2} (the blank without the complex generates 0.31 mA cm^{-2}) at a potential of 1.4 V and pH 6.0, that is 4.8 and 9.2 times higher compared to those of *d*-**3** and *p*,*p*-**Ru_2(μ-Cl)**. Importantly, the current density value (3.5 mA cm^{-2} at pH 6.0) obtained from *p*,*p*-**$Ru_2(OH)(OH_2)$** was much higher than that (1.4 mA cm^{-2} at pH 9.0) obtained for *p*,*p*-**Ru_2(μ-OH)**, under even thermodynamically unfavorable pH conditions. These results suggest that the *proximal*,*proximal*-dinuclear Ru(II) core structure with vicinal aquo and hydroxo groups is inevitably essential for efficient electrocatalytic water oxidation. Bulk electrolysis was performed in a nearly neutral phosphate buffer solution (pH 6.0) for *p*,*p*-**$Ru_2(OH)(OH_2)$** at 1.3 V vs. SCE. A higher charge amount of 2.1 C compared to the that (0.55 C) of the blank without the complex was obtained, and a 4.2 μmol (Faradaic efficiency 76–80%) of O_2 was

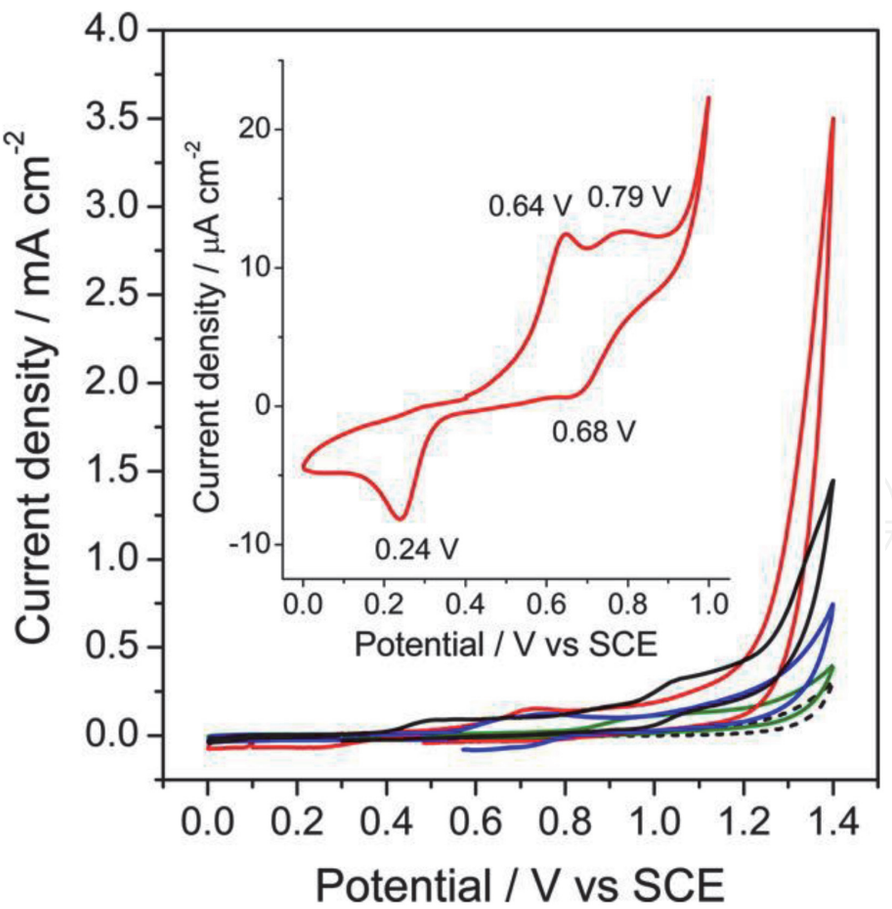

Figure 19.
CVs of 1 mM p,p-***$Ru_2(OH)(OH_2)$*** *(red),* d-***3*** *(blue),* p,p-***Ru_2(μ-Cl)*** *(green), and blank (black dots) in a 0.1 M phosphate buffer (pH 6.0) at a scan rate of 50 mV* s^{-1}*. CV of* p,p-***Ru_2(μ-OH)*** *(black) was measured at pH 9.0 because it gradually converts to* p,p-***Ru_2(μ-Cl)*** *at acidic conditions. Inset shows CV of 0.5 mM* p,p-***$Ru_2(OH)(OH_2)$*** *in a 0.1 M phosphate buffer (pH 7.0) at a scan rate of 20 mV* s^{-1}*. (Reprinted with permission from ref. [37] with permission of American Chemical Society).*

produced after 1 h electrolysis. This evolved O_2 amount obtained by ***p*,*p*-Ru$_2$(OH)(OH$_2$)** corresponds to 5.3 equivalent of the total ***p*,*p*-Ru$_2$(OH)(OH$_2$)** amount (0.6 μmol) in the electrolyte solution, ensuring the catalytic water oxidation. The UV–Visible absorption spectrum of the electrolyte solution after the electrolysis displayed an intense band at 694 nm, assigned to *proximal*,*proximal*-$[Ru^{III}{}_2(tpy)_2L(OH)_2]^{4+}$ (abbreviated to Ru^{III}-OH:Ru^{III}-OH as a oxidation state). This observation suggests that Ru^{III}-OH:Ru^{III}-OH is involved in the catalytic cycle. For the proposed electrocatalytic cycle for water oxidation under neutral conditions, ***p*,*p*-Ru$_2$(OH)(OH$_2$)** was electrochemically oxidized by the proton-coupled electron transfer reactions *via* Ru^{III}-OH:Ru^{III}-OH and Ru^{IV}=O:Ru^{IV}–OH states most possibly to the Ru^{V}=O:Ru^{V}=O state, which could oxidize water to O_2 together with the regeneration of Ru^{III}-OH:Ru^{III}-OH.

In order to provide mechanistic insights into O–O bond formation for O_2 production, the H/D isotope effect on electrocatalytic water oxidation by ***p*,*p*-Ru$_2$(OH)(OH$_2$)** and ***d*-3** were examined in H_2O and D_2O media. A large H/D isotope effect (1.7) on electrocatalytic water oxidation by ***d*-3** was observed relative to the blank experiment (1.1). This result is consistent with the proton transfer-concerted O–O bond formation by the *WNA* mechanism. On the other hand, the isotopic effect (1.1) on the electrocatalysis by ***p*,*p*-Ru$_2$(OH)(OH$_2$)** was comparable with the blank (1.1). The lower isotope effect indicates proton-non-concerted chemical reaction process in the electrocatalytic cycle, and ***p*,*p*-Ru$_2$(OH)(OH$_2$)** is likely to produce O_2 *via* the *I2M* mechanism.

4. Conclusions

Recent progress on the aspects and mechanistic insights of photoisomerization of Ru(II) aquo complexes in our group was reviewed to unveil the photoisomerization reactions and its mechanism comprehensively. The controls of properties and functions of mononuclear Ru(II) aquo complexes by the photoisomerization were exemplified in terms of their water oxidation catalyses. An example of application of the photoisomerization is demonstrated; the employment of the photoisomerization enabled to synthesize the dinuclear Ru(II) complexes that have been difficult to be synthesized by conventional thermochemical processes. The synthesized dinuclear complexes also serve as efficient catalysts for water oxidation. New design and development of variety types of Ru complexes are desired to explore unique reactions, functions and application based on the photoisomerization for future molecular systems such as artificial photosynthetic devices.

Author details

Yuta Tsubonouchi, Eman A. Mohamed, Zaki N. Zahran and Masayuki Yagi*
Department of Materials Science and Technology, Faculty of Engineering, Niigata University, Niigata, Japan

*Address all correspondence to: yagi@eng.niigata-u.ac.jp

References

[1] Thompson DW, Ito A, Meyer TJ. [Ru(bpy)$_3$]$^{2+*}$ and other remarkable metal-to-ligand charge transfer (MLCT) excited states. Pure Appl Chem 2013;85:1257–1305. https://doi.org/10.1351/PAC-CON-13-03-04.

[2] Kinoshita T, Dy JT, Uchida S, Kubo T, Segawa H. Wideband dye-sensitized solar cells employing a phosphine-coordinated ruthenium sensitizer. Nat Photonics 2013;7:535–539. https://doi.org/10.1038/nphoton.2013.136.

[3] Caspar J V., Meyer TJ. Photochemistry of tris(2,2′-bipyridine) ruthenium(2+) ion (Ru(bpy)$_3^{2+}$). Solvent effects. J Am Chem Soc 1983;105:5583–5590. https://doi.org/10.1021/ja00355a009.

[4] Hammarström L, Johansson O. Expanded bite angles in tridentate ligands. Improving the photophysical properties in bistridentate Ru^{II} polypyridine complexes. Coord Chem Rev 2010;254:2546–2559. https://doi.org/10.1016/j.ccr.2010.01.006.

[5] Winkler JR, Netzel TL, Creutz C, Sutin N. Direct Observation of Metal-to-Ligand Charge-Transfer (MLCT) Excited States of Pentaammineruthenium(II) Complexes. J Am Chem Soc 1987;109:2381–2392. https://doi.org/10.1021/ja00242a023.

[6] Abrahamsson M, Jäger M, Kumar RJ, Österman T, Persson P, Becker H-C, et al. Bistridentate Ruthenium (II)polypyridyl-Type Complexes with Microsecond ^{3}MLCT State Lifetimes: Sensitizers for Rod-Like Molecular Arrays. J Am Chem Soc 2008;130:15533–15542. https://doi.org/10.1021/ja804890k.

[7] Rillema DP, Allen G, Meyer TJ, Conrad D. Redox properties of ruthenium(II) tris chelate complexes containing the ligands 2,2′-bipyrazine, 2,2′-bipyridine, and 2,2′-bipyrimidine. Inorg Chem 1983;22:1617–1622. https://doi.org/10.1021/ic00153a012.

[8] Juris A, Balzani V, Barigelletti F, Campagna S, Belser P, von Zelewsky A. Ru(II) polypyridine complexes: photophysics, photochemistry, eletrochemistry, and chemiluminescence. Coord Chem Rev 1988;84:85–277. https://doi.org/10.1016/0010-8545(88)80032-8.

[9] Moon HC, Lodge TP, Frisbie CD. Solution-processable electrochemiluminescent ion gels for flexible, low-voltage, emissive displays on plastic. J Am Chem Soc 2014;136:3705–3712. https://doi.org/10.1021/ja5002899.

[10] Banasz R, Wałęsa-Chorab M. Polymeric complexes of transition metal ions as electrochromic materials: Synthesis and properties. Coord Chem Rev 2019;389:1–18. https://doi.org/10.1016/j.ccr.2019.03.009.

[11] Weinberg DR, Gagliardi CJ, Hull JF, Murphy CF, Kent CA, Westlake BC, et al. Proton-Coupled Electron Transfer. Chem Rev 2012;112:4016–4093. https://doi.org/10.1021/cr200177j.

[12] Pannwitz A, Wenger OS. Proton coupled electron transfer from the excited state of a ruthenium(ii) pyridylimidazole complex. Phys Chem Chem Phys 2016;18:11374–11382. https://doi.org/10.1039/c6cp00437g.

[13] Okamura M, Yoshida M, Kuga R, Sakai K, Kondo M, Masaoka S. A mononuclear ruthenium complex showing multiple proton-coupled electron transfer toward multi-electron transfer reactions. Dalton Trans 2012;41:13081–13089. https://doi.org/10.1039/c2dt30773a.

[14] Nicewicz DA, MacMillan DWC. Merging photoredox catalysis with organocatalysis: The direct asymmetric alkylation of aldehydes. Science (80-) 2008;322:77–80. https://doi.org/10.1126/science.1161976.

[15] Troian-Gautier L, Turlington MD, Wehlin SAM, Maurer AB, Brady MD, Swords WB, et al. Halide Photoredox Chemistry. Chem Rev 2019;119:4628–4683. https://doi.org/10.1021/acs.chemrev.8b00732.

[16] Poynton FE, Bright SA, Blasco S, Williams DC, Kelly JM, Gunnlaugsson T. The development of ruthenium(II) polypyridyl complexes and conjugates for: In vitro cellular and in vivo applications. Chem Soc Rev 2017;46:7706–7756. https://doi.org/10.1039/c7cs00680b.

[17] O'Regan B, Grätzel M. A low-cost, high-efficiency solar cell based on dye-sensitized colloidal TiO_2 films. Nature 1991;353:737–740. https://doi.org/10.1038/353737a0.

[18] Buda M, Kalyuzhny G, Bard AJ. Thin-Film Solid-State Electroluminescent Devices Based On Tris(2,2′-bipyridine) ruthenium(II) Complexes. J Am Chem Soc 2002;124:6090–6098. https://doi.org/10.1021/ja017834h.

[19] Concepcion JJ, House RL, Papanikolas JM, Meyer TJ. Chemical approaches to artificial photosynthesis. Proc Natl Acad Sci 2012;109:15560–15564. https://doi.org/10.1073/pnas.1212254109.

[20] Zahran ZN, Tsubonouchi Y, Mohamed EA, Yagi M. Recent Advances in the Development of Molecular Catalyst-Based Anodes for Water Oxidation toward Artificial Photosynthesis. ChemSusChem 2019;12:1775–1793. https://doi.org/10.1002/cssc.201802795.

[21] Yamazaki H, Hakamata T, Komi M, Yagi M. Stoichiometric photoisomerization of mononuclear ruthenium(II) monoaquo complexes controlling redox properties and water oxidation catalysis. J Am Chem Soc 2011;133:8846–8849. https://doi.org/10.1021/ja2024228.

[22] Hirahara M, Ertem MZ, Komi M, Yamazaki H, Cramer CJ, Yagi M. Mechanisms of photoisomerization and water-oxidation catalysis of mononuclear ruthenium(II) monoaquo complexes. Inorg Chem 2013;52:6354–6364. https://doi.org/10.1021/ic400054k.

[23] Hirahara M, Yagi M. Photoisomerization of ruthenium(II) aquo complexes: mechanistic insights and application development. Dalton Trans 2017;46:3787–3799. https://doi.org/10.1039/C7DT00079K.

[24] Durham B, Wilson SR, Hodgson DJ, Meyer TJ. Cis-Trans Photoisomerization in $Ru(bpy)_2(OH_2)_2^{2+}$. Crystal Structure of trans-$[Ru(bpy)_2(OH_2)(OH)](ClO_4)_2$. J Am Chem Soc 1980;102:600–607. https://doi.org/10.1021/ja00522a026.

[25] Durham B, Walsh JL, Carter CL, Meyer TJ. Synthetic Applications of Photosubstitution Reactions of Poly (Pyridyl) Complexes of Ruthenium(II). Inorg Chem 1980;19:860–865. https://doi.org/10.1021/ic50206a014.

[26] Pinnick D V., Durham B. Photosubstitution reactions of $Ru(bpy)_2XY^{n+}$ complexes. Inorg Chem 1984;23:1440–1445. https://doi.org/10.1021/ic00178a028.

[27] Hecker CR, Fanwick PE, McMillin DR. Evidence for Dissociative Photosubstitution Reactions of $[Ru(trpy)(bpy)(NCCH_3)]^{2+}$. Crystal and Molecular Structure of $[Ru(trpy)(bpy)(py)](PF_6)_2 \bullet (CH_3)_2CO$. Inorg Chem 1991;30:659–666. https://doi.org/10.1021/ic00004a013.

[28] Howerton BS, Heidary DK, Glazer EC. Strained ruthenium

complexes are potent light-activated anticancer agents. J Am Chem Soc 2012; 134:8324–8327. https://doi.org/10.1021/ja3009677.

[29] Albani BA, Peña B, Leed NA, De Paula NABG, Pavani C, Baptista MS, et al. Marked improvement in photoinduced cell death by a new tris-heteroleptic complex with dual action: Singlet oxygen sensitization and ligand dissociation. J Am Chem Soc 2014;136: 17095–17101. https://doi.org/10.1021/ja508272h.

[30] Porter GB, Sparks RH. Photoracemization of Ru (Bipyridine)$_3^{2+}$. J Photochem 1980;13:123–131. https://doi.org/10.1016/0047-2670(80)85004-0.

[31] Rachford AA, Rack JJ. Picosecond isomerization in photochromic ruthenium - Dimethyl sulfoxide complexes. J Am Chem Soc 2006;128: 14318–14324. https://doi.org/10.1021/ja0641305.

[32] Miyazaki S, Kojima T, Fukuzumi S. Photochemical and thermal isomerization of a ruthenium(II)-alloxazine complex involving an unusual coordination mode. J Am Chem Soc 2008;130:1556–1557. https://doi.org/10.1021/ja077954a.

[33] Bonnet S, Limburg B, Meeldijk JD, Gebbink RJMK, Killian JA. Ruthenium-decorated lipid vesicles: Light-induced release of [Ru(terpy)(bpy)(OH$_2$)]$^{2+}$ and thermal back coordination. J Am Chem Soc 2011;133:252–261. https://doi.org/10.1021/ja105025m.

[34] Hirahara M, Hakamata T, League AB, Ertem MZ, Takahashi K, Nagai S, et al. Mechanisms and Factors Controlling Photoisomerization Equilibria, Ligand Exchange, and Water Oxidation Catalysis Capabilities of Mononuclear Ruthenium(II) Complexes. Eur J Inorg Chem 2015; 2015:3892–3903. https://doi.org/10.1002/ejic.201500642.

[35] Takahashi K, Zhang X, Hirahara M, Sato T, Saito K, Yui T, et al. Influence of chloro substituent on photoisomerization, redox reactions and water oxidation catalysis of mononuclear ruthenium complexes. J Photochem Photobiol A Chem 2015;313: 117–125. https://doi.org/10.1016/j.jphotochem.2015.05.029.

[36] Tanaka S, Takahashi K, Hirahara M, Yagi M, Onda K. Characterization of the excited states of distal- and proximal-[Ru(tpy)(pynp)OH$_2$]$^{2+}$ in aqueous solution using time-resolved infrared spectroscopy. J Photochem Photobiol A Chem 2015;313:87–98. https://doi.org/10.1016/j.jphotochem.2015.06.018.

[37] Hirahara M, Nagai S, Takahashi K, Saito K, Yui T, Yagi M. New Series of Dinuclear Ruthenium(II) Complexes Synthesized Using Photoisomerization for Efficient Water Oxidation Catalysis. Inorg Chem 2015;54:7627–7635. https://doi.org/10.1021/acs.inorgchem.5b01264.

[38] Hirahara M, Nagai S, Takahashi K, Watabe S, Sato T, Saito K, et al. Mechanistic Insight into Reversible Core Structural Changes of Dinuclear μ-Hydroxoruthenium(II) Complexes with a 2,8-Di-2-pyridyl-1,9,10-anthyridine Backbone Prior to Water Oxidation Catalysis. Inorg Chem 2017;56:10235–10246. https://doi.org/10.1021/acs.inorgchem.7b00978.

[39] Yagi M, Tajima S, Komi M, Yamazaki H. Highly active and tunable catalysts for O_2 evolution from water based on mononuclear ruthenium(ii) monoaquo complexes. Dalton Trans 2011;40:3802. https://doi.org/10.1039/c0dt01826k.

[40] Watabe S, Tanahashi Y, Hirahara M, Yamazaki H, Takahashi K, Mohamed EA, et al. Critical Hammett Electron-Donating Ability of Substituent Groups for Efficient Water Oxidation Catalysis by Mononuclear

Ruthenium Aquo Complexes. Inorg Chem 2019;58:12716–12723. https://doi.org/10.1021/acs.inorgchem.9b01623.

[41] Planas N, Vigara L, Cady C, Miró P, Huang P, Hammarström L, et al. Electronic Structure of Oxidized Complexes Derived from cis-$[Ru^{II}(bpy)_2(H_2O)_2]^{2+}$ and Its Photoisomerization Mechanism Inorg Chem 2011;50:11134–42. https://doi.org/10.1021/ic201686c.

[42] Allsopp SR, Cox A, Kemp TJ, Reed WJ. Inorganic photophysics in solution. Part 1.—Temperature activation of decay processes in the luminescence of tris(2,2′-bipyridine) ruthenium(II) and tris(1,10-phenanthroline)ruthenium(II) ions. J Chem Soc Faraday Trans 1 1978;74:1275–89. https://doi.org/10.1039/f19787401275.

[43] Durham B, Caspar J V, Nagle JK, Meyer TJ. Photochemistry of $Ru(bpy)_3^{2+}$. J Am Chem Soc 1982;104:4803–4810. https://doi.org/10.1021/ja00382a012.

[44] Norrby T, Börje A, Åkermark B, Hammarström L, Alsins J, Lashgari K, et al. Synthesis, Structure, and Photophysical Properties of Novel Ruthenium(II) Carboxypyridine Type Complexes. Inorg Chem 1997;36:5850–5858. https://doi.org/10.1021/ic9705812.

[45] Li C, Hoffman MZ. Electron Localization or Delocalization in the MLCT Excited States of $Ru(bpy)_3^{2+}$ and $Ru(phen)_3^{2+}$. Consequences to Their Photochemistry and Photophysics in Fluid Solution. Inorg Chem 1998;37:830–832. https://doi.org/10.1021/ic970959w.

[46] Caspar J V, Kober EM, Sullivan BP, Meyer TJ. Application of the energy gap law to the decay of charge-transfer excited states. J Am Chem Soc 1982;104:630–632. https://doi.org/10.1021/ja00366a051.

[47] Caspar J V., Meyer TJ. Application of the energy gap law to nonradiative, excited-state decay. J Phys Chem 1983;87:952–957. https://doi.org/10.1021/j100229a010.

[48] Kober EM, Caspar J V., Lumpkin RS, Meyer TJ. Application of the energy gap law to excited-state decay of osmium(II)-polypyridine complexes: Calculation of relative nonradiative decay rates from emission spectral profiles. J Phys Chem 1986;90:3722–3734. https://doi.org/10.1021/j100407a046.

[49] Li S, Cooper VR, Thonhauser T, Puzder A, Langreth DC. A Density Functional Theory Study of the Benzene−Water Complex. J Phys Chem A 2008;112:9031–9036. https://doi.org/10.1021/jp801693p.

[50] Masaoka S, Sakai K. Clear Evidence Showing the Robustness of a Highly Active Oxygen-evolving Mononuclear Ruthenium Complex with an Aqua Ligand. Chem Lett 2009;38:182–183. https://doi.org/10.1246/cl.2009.182.

[51] Concepcion JJ, Jurss JW, Templeton JL, Meyer TJ. One site is enough. Catalytic water oxidation by $[Ru(tpy)(bpm)(OH_2)]^{2+}$ and $[Ru(tpy)(bpz)(OH_2)]^{2+}$. J Am Chem Soc 2008;130:16462–16463. https://doi.org/10.1021/ja8059649.

[52] Wasylenko DJ, Ganesamoorthy C, Henderson MA, Koivisto BD, Osthoff HD, Berlinguette CP. Electronic modification of the $[Ru^{II}(tpy)(bpy)(OH_2)]^{2+}$ scaffold: Effects on catalytic water oxidation. J Am Chem Soc 2010;132:16094–16106. https://doi.org/10.1021/ja106108y.

[53] Meyer TJ, Sheridan M V., Sherman BD. Mechanisms of molecular water oxidation in solution and on oxide surfaces. Chem Soc Rev 2017;46:6148–6169. https://doi.org/10.1039/C7CS00465F.

[54] Kärkäs MD, Verho O, Johnston E V., Åkermark B. Artificial Photosynthesis: Molecular Systems for Catalytic Water Oxidation. Chem Rev 2014;114:11863–12001. https://doi.org/10.1021/cr400572f.

[55] Garrido-Barros P, Gimbert-Suriñach C, Matheu R, Sala X, Llobet A. How to make an efficient and robust molecular catalyst for water oxidation. Chem Soc Rev 2017;46:6088–6098. https://doi.org/10.1039/c7cs00248c.

[56] Shaffer DW, Xie Y, Concepcion JJ. O–O bond formation in ruthenium-catalyzed water oxidation: single-site nucleophilic attack vs. O–O radical coupling. Chem Soc Rev 2017;46:6170–6193. https://doi.org/10.1039/C7CS00542C.

[57] Matheu R, Ertem MZ, Benet-Buchholz J, Coronado E, Batista VS, Sala X, et al. Intramolecular Proton Transfer Boosts Water Oxidation Catalyzed by a Ru Complex. J Am Chem Soc 2015;137:10786–10795. https://doi.org/10.1021/jacs.5b06541.

[58] Schulze M, Kunz V, Frischmann PD, Würthner F. A supramolecular ruthenium macrocycle with high catalytic activity for water oxidation that mechanistically mimics photosystem II. Nat Chem 2016;8:576–583. https://doi.org/10.1038/nchem.2503.

[59] Wada T, Ohtsu H, Tanaka K. Catalytic four-electron oxidation of water by intramolecular coupling of the oxo ligands of a bis(ruthenium-bipyridine) complex. Chem - A Eur J 2012;18:2374–2381. https://doi.org/10.1002/chem.201102236.

[60] Romain S, Bozoglian F, Sala X, Llobet A. Oxygen-oxygen bond formation by the Ru-Hbpp water oxidation catalyst occurssolely via an intramolecular reaction pathway. J Am Chem Soc 2009;131:2768–2769. https://doi.org/10.1021/ja808166d.

[61] Duan L, Bozoglian F, Mandal S, Stewart B, Privalov T, Llobet A, et al. A molecular ruthenium catalyst with water-oxidation activity comparable to that of photosystem II. Nat Chem 2012;4:418–423. https://doi.org/10.1038/nchem.1301.

[62] Maji S, Vigara L, Cottone F, Bozoglian F, Benet-Buchholz J, Llobet A. Ligand geometry directs O-O bond-formation pathway in ruthenium-based water oxidation catalyst. Angew Chemie - Int Ed 2012;51:5967–5970. https://doi.org/10.1002/anie.201201356.

[63] Bard, A. J., ed., Encyclopedia of Electrochemistry of the Elements, Marcel Dekker, Inc., 1973. n.d.

[64] Hansch C, Leo A, Taft RW. A survey of Hammett substituent constants and resonance and field parameters. Chem Rev 1991;91:165–195. https://doi.org/10.1021/cr00002a004.

[65] Kagalwala HN, Tong L, Zong R, Kohler L, Ahlquist MSG, Fan T, et al. Evidence for Oxidative Decay of a Ru-Bound Ligand during Catalyzed Water Oxidation. ACS Catal 2017;7:2607–2615. https://doi.org/10.1021/acscatal.6b03278.

[66] Liu Y, Chen G, Yiu S-M, Wong C-Y, Lau T-C. Intermediates in the Oxidative Degradation of a Ruthenium-Bound 2,2′-Bipyridyl-Phenoxy Ligand during Catalytic Water Oxidation. ChemCatChem 2018;10:501–504. https://doi.org/10.1002/cctc.201701319.